STUDY ON FLOW STRUCTURE BEHIND MULTIPLE BLUFF BODIES IN A TANDEM ARRANGEMENT IN A CHANNEL UNDER THE EFFECT OF A MAGNETIC FIELD

BY

NUR MARISSA BINTI KAMARUL BAHARIN

A dissertation submitted in fulfillment of the requirement for
the degree of Master of Science in Engineering

Kulliyyah of Engineering
International Islamic University Malaysia

FEBRUARY 2023

ABSTRACT

Nuclear fusion is one of the future solutions towards sustainable energy. The concept of the magnetic field is introduced to contain high-temperatureture reaction of the nuclear fusion. However, the presence of the magnetic field influences the flow of fluid within the blanket module, which purpose is to harness the energy. This has the effect of reducing the efficiency of heat transfer through the channel of a heat exchanger. Thus, to counter this effect, this research investigates the flow structure behind multiple bluff bodies arranged in tandem in a channel under the influence of a magnetic field in the pursuit of increasing the heat transfer efficiency inside the channel. In this study, the effect of gap ratio, G/h = [1-2.4] and Hartmann parameters, H = [0-800] are analyzed for the critical Reynolds number, pressure drop and Nusselt number using a Computational Fluid Dynamics open-source software. It is found that the presence of the downstream cylinder with gap ratio, G/h = 1.2, 1.4 and 1.6 improves the flow in terms of critical Reynolds number and Nusselt number while having some pressure drop penalty. The multiple cylinders increased the Nusselt number compared with the flow past a single cylinder. In terms of the Hartman parameter, increasing the value of the parameter increases the critical Reynolds number and decreases the Nusselt number.

الخلاصة

الإندماج النووي هو أحد الحلول المستقبلية للطاقة المستدامة مّما يشيد بأهّميّة مفهوم المجال المغناطيسي من أجل إحتواء تفاعل درجة الحرارة العالية للانصهار النووي. ومع ذلك، فإنّ المجال المغناطيسي يؤثر على تدفّق السّوائل داخل وحدة البطانية والذي يعتبر الغرض منه هو تسخير الطاقة، حيث يقلل المجال المغناطيسي من كفاءة نقل الحرارة في قناة المبادل الحراري. في سبيل مواجهة هذا التأثير، فإنّ هذا البحث يفحص هيكل التدفّق وراء مجموعة من الأجسام الغير إنسيابيه الشكل و مرتبة جنباً إلى جنب في داخل القناة تحت تأثير مجال مغناطيسي بهدف زيادة كفاءة نقل الحرارة داخل القناة. في هذه الدراسه تم تحليل تأثير نسبة الفراغ(١-٢.٤) و متغير هارتمان(٠.٨٠٠)، على رقم رينولدز الحرج وانخفاض الضغط بالإضافة إلى رقم نسلت بواسطة برنامج تحليل ديناميكية الموائع الحسابيه. ومن النتائج، وجد أن إسطوانة المصبّ بنسبة فراغ ١.٢ ، ١.٤ و ١.٦ يحسّن التدفق من حيث رقم رينولدز الحرج ورقم نسلت و أدّت الأسطوانات المتعددة إلى زيادة رقم نسلت مقارنةً بالتدفق الذي يتجاوز أسطوانة واحدة. فيما يتعلق بمتغيّر هارتمان ، تؤدّي زيادة قيمة المتغيّر إلى زيادة رقم رينولدز الحرج وتقليل رقم نسلت.

APPROVAL PAGE

I certify that I have supervised and read this study and that in my opinion, it conforms to acceptable standards of scholarly presentation and is fully adequate, in scope and quality, as a thesis for the degree of Master of Science in Engineering

………………………………….
Mohd Azan Mohammed Sapardi
Supervisor

………………………………….
Syed Noh Syed Abu Bakar
Co-Supervisor

I certify that I have read this study and that in my opinion it conforms to acceptable standards of scholarly presentation and is fully adequate, in scope and quality, as a thesis for the degree of Master of Science in Engineering

……………………………….

Amelda Dianne Binti Andan
Examiner

……………………………….

Azlin Binti Mohd Azmi
External Examiner

This thesis was submitted to the Department of Mechanical and Aerospace Engineering and is accepted as a fulfilment of the requirement for the degree of Master of Science in Engineering

…………………………….

Fadly Jashi Darsivan Bin Ridhuan Siradj
Head, Department of Mechanical and Aerospace Engineering

This thesis was submitted to the Kulliyyah of Engineering and is accepted as a fulfillment of the requirement for the degree of Master of Science in Engineering

…………………………….

Sany Izan Ihsan
Dean of Kuliyyah of Engineering

DECLARATION

I hereby declare that this thesis is the result of my own investigations, except where otherwise stated. I also declare that it has not been previously or concurrently submitted as a whole for any other degrees at IIUM or other institutions.

Nur Marissa Binti Kamarul Baharin

Signature…………………………   Date……………………… 1 February 2023

INTERNATIONAL ISLAMIC UNIVERSITY MALAYSIA

DECLARATION OF COPYRIGHT AND AFFIRMATION OF FAIR USE OF UNPUBLISHED RESEARCH

STUDY ON FLOW STRUCTURE BEHIND MULTIPLE BLUFF BODIES IN A TANDEM ARRANGEMENT IN A CHANNEL UNDER THE EFFECT OF A MAGNETIC FIELD

……………………………	1 February 2023
Signature	…………………..
	Date

This thesis is dedicated to my parents for laying the foundation of what I turned out to

be in life.

ACKNOWLEDGEMENTS

Foremost, I would like to express my sincere gratitude to my supervisor Dr. Mohd Azan Bin Mohammed Sapardi for his patience, motivation, enthusiasm, immense knowledge, and for being the first to introduce to me the world of research. His guidance helped me in all the time of this research and the writing of this report. I could not have imagined having a better role model and mentor for this project. I am also grateful to my co-supervisor, Asst. Prof. Dr. Syed Noh Bin Syed Abu Bakar, whose support and cooperation contributed to the outcome of this work.

My sincere gratitude also goes to my dearest significant other, who have been supporting, tolerating, and sustaining me during the period of this project. Thank you for the encouragement given at all times and the faith that I can finish this research.

Last but not least, to my family, starting from my parents to my brother and sisters, who have been giving me warm love and support from the commencement of the study. You have been my source of laughter, joy, backbones, and pride. For that, I can never thank all of you enough.

TABLE OF CONTENTS

LIST OF ABBREVIATIONS

HD	Hydrodynamics
MHD	Magnetohydrodynamics
d	Diameter
G	Gap length between bluff bodies
G/h	Gap Ratio
H	Hartmann friction parameter
h	Height of channel
Ld	Downstream Length
Lu	Upstream Length
Pr	Prandtl number
Re	Reynolds number
Re_c	Critical Reynolds number
St	Strouhal number
t	time
U	Velocity
V	Kinematic viscosity
β	Blockage Ratio
U	Steady two-dimensional flow velocity
u	Velocity vector
u	x-direction velocity component
v	y-direction velocity component

w	z-direction velocity component
τ	stress
ρ	Fluid density
F_L	Lift force
C_L	Lift coefficient
T	Diffusivity
Nu	Nusselt number
Nu_w	Local Nusselt number along bottom heated wall
θ	Temperature field
θ_f	Bulk fluid temperature
θ_w	Local wall fluid temperature
P	Pressure
p	Kinematic pressure field

LIST OF FIGURES

CHAPTER ONE

INTRODUCTION

1.1   BACKGROUND OF STUDY

1.1.1   Magnetohydrodynamics

Electrically conducting fluids (magnetofluids), have their own behavior and magnetic properties. According to Singh (2017), the study of the magnetofluid, with respect to its behavior and magnetic properties, is known as magnetohydrodynamics or hydromagnetics.

The history of magnetohydrodynamics dates back to the 1940s when this branch of physics was first discovered by Swedish Physicist Hannes Alfvèn (Davidson, 2002). Hannes Alfvèn, won a Noble Prize in Physics as he was the pioneer in the field of magnetohydrodynamics (MHD).

Though it was not officially recorded under magnetohydrodynamics (MHD), the first experiment was, however, first conducted in 1832 by Michael Faraday (Malghan, 1996), where he called this effect "magneto-electric induction". Faraday attempted to determine the potential difference induced by the flow across the Thames River and the magnetic field of the Earth to determine the velocity of the flow. The experiment was not a success. But later, his invention of the electromagnetic flowmeter (Shercliff, 1962) made an impact today as it has contributed a lot and is vital in many industries.

1.2.1 Magnetohydrodynamics in Plasma Fusion Reactor

Studies pertaining to this matter were not as extensive before as it is now, but in order to create sustainable energy, more thesis and research studies are emerging to apply MHD to the existing problems. Some of the studies on MHD flow were done by Hussam et al. (2011, 2012a, 2012b, 2013), Hamid et al. (2015, 2016) and Sapardi et al. (2014, 2015).

International Thermonuclear Experimental Reactor (ITER) project introduces the first fusion facility to generate energy using the concept of MHD to create a plasma fusion reactor in 2005. The reactor confined a superheated plasma of hydrogen ions, namely Deuterium and Tritium, inside a magnetic field in a donut shape torus called a Tokamak. According to Mirnov (2018), the evolution of Tokamak started in late 1962, when it was first developed by Soviet Research under the leadership of academician L.A. Artsimovich. Later, as the more promising configuration of the magnetic fusion device, the Tokamak has been adopted worldwide. The largest Tokamak is under progress through the ITER project, where it will be twice as large as the biggest machine currently in service, and ten times the volume of the plasma chamber.

Though to Hussam and Sheard (2013), MHD flow in rectangular ducts has its own significance in metallurgical processing applications; however, the effect of MHD in the fusion blanket has to be avoided. However, the MHD effect in the fusion blanket must be avoided. The flow can conveniently be caused to laminarize by the steady strong magnetic field, (Moffatt 1967; Branover 1978; Mutschke et al. 1997) which may further decrease the effectiveness of the heat transfer from the fusion blanket. According to Zikanov et al. (2014), a magnetic field applied on the flow of an electrical conductive fluid can immensely alter the behaviour of the flow. This effect is seen in the laminar-turbulent transition situation in magnetohydrodynamics flow inside pipe, duct, and channel flows with the influence of magnetic field. All the studies (Moffatt 1967; Branover 1978;

Mutschke et al. 1997; Zikanov et al. 2014) show that MHD has an impact on flow behavior.

1.2 PURPOSE OF THE STUDY

The purpose of this study is to understand the flow past bluff bodies in a tandem arrangement in MHD complication in comparison to the flow past a single bluff body over the Reynolds number, pressure drop and Nusselt number. To further narrow down on a specific discussion, the behavior of conducting fluid is studied by placing two circular cylinder bluff bodies in a tandem arrangement so that the flow can transition from a steady to an unsteady state. Unsteady flow is essential in increasing the efficiency of heat transfer because it will improve the mixing of cold and hot fluids.

To support the study, it is keen to investigate the problem over a study parameter like the gap between bluff bodies.

1.3 PROBLEM STATEMENT

As a promising option to become the world's primary source of energy, the idea of plasma fusion is adapted to make up for toxic fossil fuels, nuclear waste and etc. The plasma fusion aligns well with Sustainable Development Goals number seven which is 'Affordable and Clean Energy'. Therefore, in order to support the vision, the problem that arises due to the effect of the magnetic field in the fusion blanket of the plasma fusion reactor must be overcome so that abundant energy can be harnessed from the fusion reactor.

According to Dobran (2012), the most technologically advanced machine built is the International Thermonuclear Experimental Reactor (ITER), where net energy from fusion is expected to be produced. However, the discussion is still open regarding the plasma confinement, heat removal, fuel supply and reactor materials. The efficiency of heat transfer in the fusion blanket with magnetic field effect is, therefore, of great technological pertinence, and in this paper, the behavior of the

fluid flow and its ability to transfer heat under the effect of the magnetic field is addressed.

The MHD affects the fluid flow where the flow structure becomes steady and thus decreases the heat efficiency in the fusion blanket. Therefore, the problem that arises due to the presence of the magnetic field in the fusion blanket of the plasma fusion reactor must be overcome. This research is done by including bluff bodies in tandem arrangement inside the channel to create unsteady flow. Thus, the flow structure and heat transfer are then studied with the effect of the magnetic field.

1.4   RESEARCH OBJECTIVES

The aim of this study is to investigate the flow inside the channel of the heat exchanger behind bluff bodies in a tandem arrangement and under the effect of the magnetic field. A few objectives are built upon to support the aim of this study.

The specific objectives of the study are to determine the effect of gap length and the Hartmann parameter on the critical Reynolds number (The threshold Reynolds number where the flow transitioned from steady to unsteady flow), pressure drop, and the heat transfer efficiency. Over which all of the results will be compared with the results of the flow past singular cylinder.

1.5   SCOPE OF THE RESEARCH

This research will focus on including bluff bodies in a channel as a vortex promoter in a tandem manner and determining the optimal gap length, which will cause a steady flow to change its behavior to unsteady. Past studies have been made regarding cylindrical bluff bodies. The addition in this research is the gap length between the two cylindrical bluff bodies vortex promoters. The geometry meshes and simulations for this study will be carried out using Gmsh and OpenFOAM.

1.6   DELIMITATIONS AND ASSUMPTIONS

Several parameters are used as delimiting factors in this study to define the parameters, whereby the delimiting factors are referred from the thesis of Sapardi (2018) and are used as guidelines. The non-dimensional analysis is applied to this research problem. The blockage ratio, β, is in the range of [0.1, 0.3], Hartmann parameter, $H = [0,800]$ and $Re = [1,2500]$ depending on the aims of the studies. Since the condition of the quasi-two-dimensional condition that was established by Sommeria and Moreau (1982) and Poth'erat et al. (2002) is satisfied, the MHD flow in this research is assumed to be quasi-two-dimensional, and using the Prandtl number, $Pr = 0.022$. This Prandtl number is representative of Galinstan (GalnSn) liquid metals for heat transfer studies.

1.7   THESIS ORGANIZATION

The thesis is segregated into five distinct chapters. After the initial introduction, Chapter 2 enlightens a review of relevant literature of preceding works. Chapter 3 discuss the numerical methodologies applied in this research work. Results are then presented in Chapter 4. Breaking down chapter 4, subchapter 4.1 lays out the mesh and domain dependency study. Subchapter 4.2 validates the numerical methodologies. Subchapter 4.3 investigates the impact that the gap ratio and Hartmann parameter brings on the critical Reynolds number. Subchapter 4.4 studies the effect of the gap ratio and Hartmann parameter on pressure drop. Subchapter 4.5 presents the effect of the gap ratio and Hartmann parameter on the Nusselt number. Conclusions are presented in Chapter 5.

CHAPTER TWO

LITERATURE REVIEW

2.1   INTRODUCTION

A review of the relevant literature related to nuclear fusion, fusion cooling blanket, magnetohydrodynamics (MHD) and its effect on the cooling blankets, heat Transfer of magnetohydrodynamics flow, flow past bluff bodies, vortex promoter, and vortex promoter in a channel of two circular cylinders are presented in this chapter.

2.2   NUCLEAR FUSION

The research of nuclear fusion started back in 1950 when it was conducted by scientists at that time where they formulated the principles of magnetic containment of high temperature plasmas which would allow the development of a thermonuclear reactor (Smirnov, 2009). Conceptually, the sun shines because of nuclear fusion (Fiorentini, Ricci, Villante, 2004), which leads to the fact that fusion is a thermonuclear process of very high temperature. The primary source of solar energy, and also stars of similar sizes, is the fusion of hydrogen to form Helium. Reflecting on the sun has an abundance of energy, the concept is captured.

It has been said by Sapardi (2018) that the collision between deuterium and tritium nuclei of hydrogen ions causes the fusion reaction, which produces energy and helium 5. Helium 5 splits into Helium 4 and a free neutron, which both release additional energy. (See Figure 2.1)
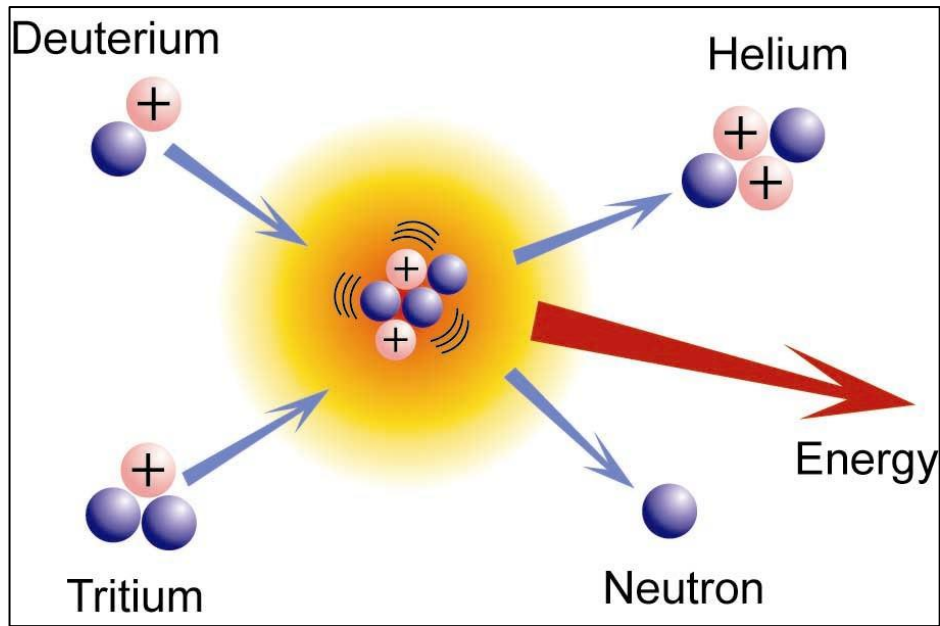
Figure 2.1 Energy, Helium and neutron is produced from the collision of Deuterium and Tritium of Hydrogen ions, also called the fusion reaction.

2.3   FUSION COOLING BLANKET

The fusion of the nuclei happens when the temperature of the fuel is extremely heated to circa 150 million degrees Celsius, forming hot plasma (Shivali, 2017). To keep the plasma away from the walls, a strong magnetic field is used as confinement so that it does not cool down and lose its energy potential. Magnetic fields generated by superconducting coils outside of a vacuum vessel keep the fusion reaction contained within the torus (Dobran 2012). This is shown in Figure 2.2 The Tokamak fusion reactor is designed where

Plasma has to be confined long enough for energy production and for fusion to occur. The intenal walls of the vacuum vessel is completely covered by the blanket modules that will Protect the structure of the steel and the superconducting toroidal field magnets from high temperature and high-energy neutrons resulting from the fusion reactions. When neutrons are slowed down in the blanket, the transformation from kinetic energy into heat energy occurs and will be collected by water coolant, where the energy that is harnessed will be used for power generation (Refer Figure 2.3).
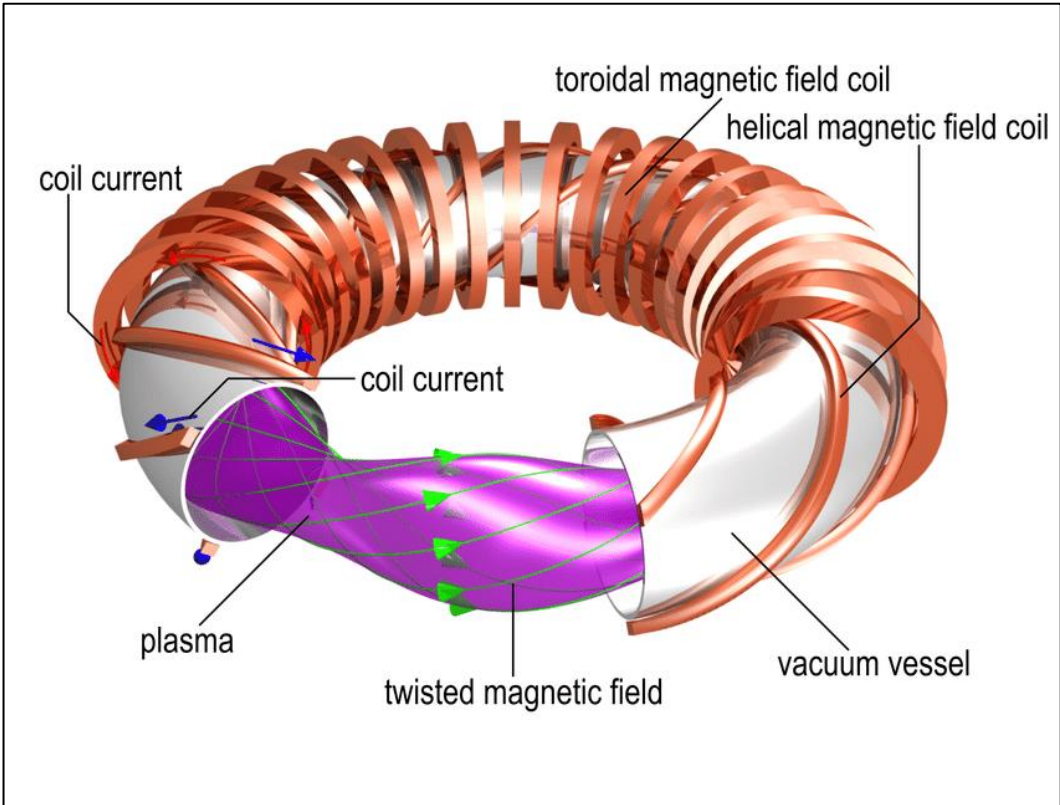
Figure 2.2 The Tokamak fusion reactor is designed where a metal blanket with self-cooling properties surrounds the plasma, which is contained in the shape of a torus.
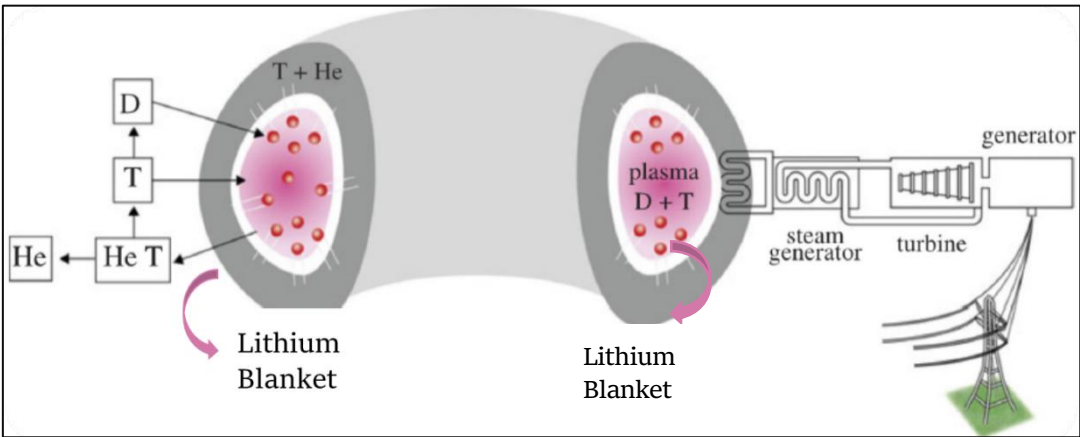
Figure 2.3 The blanket covering the fusion reaction that is connected to the generator.

2.4 MAGNETOHYDRODYNAMICS (MHD) AND ITS EFFECT TO THE COOLING BLANKETS

The presence of MHD rectangular ducts with the presence of a transverse magnetic field, is often seen in metallurgical processing applications, and within the cooling blankets enclosing magnetic confinement fusion reactors (Hussam and Sheard, 2013). The magnetic field will affect the flow inside the duct, causing the flow instabilities. Induced currents in the fluid interact with the magnetic field to create Lorentz forces, which have a significant impact on the flow pattern. (Mucks et al. 2000). Under the influence of magnetic field, the electrically conducting fluid interacts with the applied magnetic field in such a way that disturbances parallel to the magnetic field are suppressed, making the vortices to be stretched out and align parallel with the magnetic field (Sommeria & Moreau 1992; Sommeria & Moreau 1998). To further prove the effect of the magnetic field, a study was made by Ben Hadid et al. (1997), where they investigated the flow structures in a rectangular cylinder filled with liquid of electrically conducting properties when it is exposed to a constant magnetic field. From which the result shows that the magnetic field stabilizes the flow, where the flow is unstable at first and then modifies the instability nature. Currents are induced by the magnetic field's interaction with moving liquid metal.

2.5 HEAT TRANSFER OF MAGNETOHYDRODYNAMIC FLOW

Based on the article written by Chatterjee, Mondal and Hui (2013), the heat transfer rate is found to be almost unvarying at low Reynold's number, whereas it increases moderately for higher Reynold's number with the applied magnetic field. Therefore, to increase the rate of heat transfer, the Reynolds number must be increased, and this is somewhat of an obstacle because the magnetic field stabilizes the flow where the flow is first unstable. The heat transfer in a duct is then can be improved by having turbulence or an unsteady flow structure. Sapardi (2018) said that the Lorentz force from the confinement field decreases the head losses as tt has the tendency to suppress the metal flow into a laminar state in the blanket.

Based on the studies made by Singh and Gohil (2019), it is said that when the magnetic field's effect on Lorentz force and its direction are studied, it is deduced that the magnetic field transverse to the surface of the wall produces a higher Lorentz force as compared to the case of when the magnetic field is in parallel direction. The repression of heat transfer is, therefore, more in the case of the transverse magnetic field rather than parallel. The Lorentz force has the effect of suppressing the movement of the fluid inside the channel and consequently demotes heat transfer. Whereby Singh and Gohil (2019) further stated that the damping fluid motion and convective heat transfer with regards to the force are said to be more in the case of the direction of the fluid. This simply shows that heat transfer is therefore affected by the magnetic field due to the induced Lorentz force that acts in the opposite direction of the fluid flow that, causes the oscillation wave to be stretched and dampened in a quasi-two-dimensional mode.

2.6 FLOW PAST BLUFF BODIES

The interest in this topic of discussion emerged from its practice in a variety of applications in the engineering field and also the need to understand such behavior so that it can be adapted to suit certain implementations. According to Mittal and Kumar (2001), the flow past a stationary single circular cylinder, by itself, is associated with high density vortex dynamics, and significantly non-identical flow patterns are observed for various regimes of Reynolds numbers. However, when the duct is associated with two cylinders, under a tandem arrangement of the cylinders, a large amplitude oscillation is shown for the downstream cylinder (Mittal & Kumar, 2001).

According to Cassells, Hussam and Sheard (2016), in the fusion application, a net power balance analysis shows that the heat transfer enhancement has a high influence over the pumping power cost to produce net benefits for even moderate heat transfer enhancement when the flow past over a vortex promoter. This is due to the fact that separation occurs when fluid flows over a body, where it causes period

shedding of vortices to occur (Verma & Govardhan, 2011) and further causes the flow to become unsteady. Thus, in order to develop an efficient system where the heat transfer is enhanced so that power can be reduced, it is a good alternative to introducing a vortex promoter in the fluid flow. The efficiency is increased internally rather than having to exert extra external force or power to further increase the rate of heat transfer in a system.

2.7   VORTEX PROMOTER

According to Verma and Govardhan (2011), a separation may occur when a fluid flows over a body, depending on its shape and other parameters, which it can cause period shedding of vortices to occur from the body.

The phenomena may be desirable for some instances, but nevertheless, a deep comprehension of the flow field is required. Hence, vortex shedding has been an active area of research. In 1993, Roshko made a remark regarding the complexity of bluff bodies, "the problem of bluff body flow remains almost entirely in the empirical, descriptive realm of knowledge". However, the knowledge possessed by this flow is boundless.

Among many shapes of bluff bodies, the circular section has been given a considerable amount of attention by researchers due to its vast use in engineering applications such as pipelines system and heat exchangers tubes, or maybe due to the fact that the simple geometry made it easy for analysis and simulation, and partly because flow over circular cylinder comprises all of the important aspects of bluff body flow.

The interference effect causes several changes in the fluid structure's characteristics when multiple cylinders are added to a fluid flow stream. Studies of the flow around two cylindrical bluff bodies can give a clearer understanding of the vortex dynamics (Verma & Govardhan, 2011).

According to Williamson (1996), there have been sunstantial amount of papers on the case of a single circular cylinder wake alone. So the vortex dynamics phenomena, with two or multiple circular cylinders over a wide range of Reynolds numbers, is still an open subject.

The increasing number of Von Karman vortices also indirectly leads to more effective heat transport (Meis et al., 2010). From a study made by Hussam et al. (2018), a statement is deduced whereby the resulting wake and its interactions with the heated wall are relatively linked to the improvement in heat transfer. The study is a comparison of three different geometrical shapes of promoters, which are rectangular, circular and triangular. Following the heat transfer gain, it is governed by the relationship between the size, spacing, intensity, and nature of the vortices that are generated. Though the study suggests that for a duct flow under the influence of a strong magnetic field, the obstacle of a triangular shape is a fine geometry promoter for heat transfer compared to the circular cylinders or square, though the pressure drop is high.

2.8   VORTEX PROMOTER IN A CHANNEL OF TWO CIRCULAR CYLINDER

A study was made by Ayli and Bayer (2019), where it was deduced that higher blockage ratios would lead to a remarkably higher heat transfer coefficient. When the distance between the bodies increases, the shedding gains strength and thus, more turbulence will be created.

Earlier, a study is made by Assi (2010) on how two identical cylinders responded when subjected to flow interference. The findings demonstrate that the high-amplitude vibrations seen on the second cylinder are driven primarily by the vortices created by the upstream wake. In fact, when compared to the response of an isolated cylinder, the downstream cylinder of a tandem pair bluff body is known to have an augmented increment. (Assi, 2014).

Two possible arrangement exists for the two circular cylinders, which are tandem and staggered. But according to Mital and Kumar (2011), who did a study on the two arrangements, it is found that for staggered arrangement, the downstream cylinder responds like an isolated cylinder in almost all the cases, while very large amplitude oscillations are observed for the second cylinder in a tandem arrangement.

To conclude, based on all the literature review that has been made, the studies show that the magnetic field will affect the flow structure by stabilizing the flow, which reduces the Reynolds number. When the Reynolds number decreases, the heat efficiency decreases as well. To promote unsteady flow, bluff bodies can be added to the channel to increase the Reynolds number. Most of the studies are made on circular cylinder bluff bodies, and adding two circular cylinders as bluff bodies in the channel, increases the unsteadiness even more. To finalize the setup, an arrangement for the cylinder must be chosen whether to settle on a tandem or staggered arrangement. The staggered arrangement causes the second cylinder to behave like an isolated cylinder which beats the purpose of adding the second bluff body. In terms of unsteadiness, the tandem arrangement is preferred as an enormous amplitude of oscillations can be observed.

CHAPTER THREE

METHODOLOGY

3.1 FLOWCHART METHODOLOGY

The steps necessary to achieve the objectives of this study are outlined in the planning flow chart below (Refer Figure 3.1);

Framing the Research	• Identify problem • Set research boundary and scope • Identify the research methodology
Validation	Validation of results from previous paper for single cylinder using OpenFOAM

Flow pass single circular cylinder	Manipulated Variable:
	   Hartmann friction term
	
	Responding Variable :
	   Re_c, Pressure Drop, Heat Transfer Efficiency

Flow pass two circular cylinder	Manipulated Variable:
	   Gap Ratio, Hartmann Friction Term
	
	Responding Variable:
	   Re_c, Pressure Drop, Heat Transfer Efficiency

Result Comparison and Data Analysis	• Re_c, Pressure Drop, and Heat Transfer Efficiency are compared for both flow pass single circular cylinder and flow pass two circular cylinder. • The most optimized arrangement is determined for the flow past multiple bluff bodies (two circular

Figure 3.1 Flowchart planning to conduct the research study.

3.2 GOVERNING EQUATIONS

3.2.1 Navier-Stokes Equation

Navier-Stokes equations govern for viscous, heat conducting fluid. The vector equation is obtained by applying Newton's Second Law of Motion to a fluid element, where it is also called the momentum equation. The Navier-Stokes equations are supplemented by the mass conservatiosn equation (the continuity equation) (Equation 3.1) and the momentum equation (Equation 3.2) written as

$$\frac{D\rho}{dt} + \rho\nabla.\boldsymbol{u} = 0 \qquad\qquad 3.1$$

where ρ denotes density, t denotes time and **u** the flow velocity vector. An incompressible fluid will satisfy the condition which is $\nabla.\boldsymbol{u} = 0$.

$$\rho\frac{Du}{Dt} = -\frac{\partial p}{\partial x} + \frac{\partial \tau_{xx}}{\partial x} + \frac{\partial \tau_{yx}}{\partial y} + \frac{\partial \tau_{zx}}{\partial z} + \rho f_x \qquad\qquad 3.2$$

$$\rho\frac{Dv}{Dt} = -\frac{\partial p}{\partial y} + \frac{\partial \tau_{xy}}{\partial x} + \frac{\partial \tau_{yy}}{\partial y} + \frac{\partial \tau_{zy}}{\partial z} + \rho f_y \qquad\qquad 3.3$$

$$\rho\frac{Dw}{Dt} = -\frac{\partial p}{\partial z} + \frac{\partial \tau_{xz}}{\partial x} + \frac{\partial \tau_{yz}}{\partial y} + \frac{\partial \tau_{zz}}{\partial z} + \rho f_z \qquad\qquad 3.4$$

where (x, y, z) is the coordinates, (u, v, w) is the velocity components, and p is pressure. The Navier-Stokes equations in modern notation is expressed as

$$\rho\left(\frac{\partial \boldsymbol{u}}{\partial t} + \boldsymbol{u}.\nabla\boldsymbol{u}\right) = -\nabla p + \nabla.\mathrm{T} + \mathrm{f} \qquad\qquad 3.5$$

where term $\frac{\partial \boldsymbol{u}}{\partial t}$ is the change of velocity with time, $\boldsymbol{u}.\nabla\boldsymbol{u}$ is convective term, ∇p is pressure gradient, f is body force term (external forces that acts on the fluid), and $\nabla.\mathrm{T}$ is diffusion term.

In this study, the fluid is incompressible. Reflecting Newton's Second Law of Motion, this equation can be considered similar whereby the left side of the equation is the acceleration of a small region of fluid and the right side is the force acting on the fluid such as internal body surfaces, stress and pressure, as below

$$\frac{\partial \boldsymbol{u}}{\partial t} + (\boldsymbol{u} \cdot \nabla)\boldsymbol{u} = -\nabla p + \frac{1}{Re}\nabla^2 \boldsymbol{u} \qquad\qquad 3.6$$

where Re in equation 3.6 represents the ratio between internal and viscous forces. The above equation resulted in a non-dimensional form and the condition is for an incompressible fluid. Reynold's number is the contributing or controlled parameter in this equation, as it controls the outcome of values for all the other variables with the condition that the other parameters are constant.

3.2.2 SM-82 EQUATION

Magnetohydrodynamic flow is governed by Equation 3.6, for a quasi-2D model. Sommeria and Moreau proposed this model in 1982 (Sommeria & Moreau, 1982) where the flow is assumed to be incompressible and laminar. A two-dimensional approximation of the MHD flow is obtained by averaging the flow quantities in the core flow and the Hartmann layers. Equation 3.7 can be used to solve Hydrodynamic cases, as well as Magnetohydrodynamic cases.

$$\frac{\partial \boldsymbol{u}}{\partial t} = -(\boldsymbol{u} \cdot \nabla)\boldsymbol{u} - \nabla p + \frac{1}{Re}\nabla^2 \boldsymbol{u} - \frac{H}{Re}\boldsymbol{u} \qquad\qquad 3.7$$

where, u = velocity, p = pressure, H = Hartmann friction term represents the effect of the Lorentz force on the flow and it is defined as

$$H = n\left(\frac{d^2}{a}\right)Ha \qquad\qquad 3.8$$

where n is the number of Hartmann layers in the flow and in present work n = 2. For the Hartmann number, *Ha,* it represents square root of the electromagnetic force and the viscous force and is defined as

$$Ha = aB\sqrt{\left(\frac{\sigma}{\rho u}\right)} \qquad\qquad 3.9$$

where *a* and *B* denotes the applied magnetic field strength and the magnetic permeability of the fluid.

Equation 3.7 can be used to solve Hydrodynamic cases, as well as Magnetohydrodynamic cases. When the spanwise magnetic field, *B* is absent for the hydrodynamic problem, it resulted in *Ha* = 0 that leads to *H* = 0, which will regress equation (3.7) into hydrodynamic Navier–Stokes equation (Equation 3.6).

3.2.3 Energy Equation

The energy equation in Equation 3.8 is the mathematical formulation of the law of conservation of energy. Since this study is made based on dimensionless solution, thus it is keen to use dimensionless energy equation as well.

$$\frac{d\theta}{dt} + (\boldsymbol{u} \cdot \nabla)\theta = \frac{1}{Pr\,Re}\nabla^2\theta \qquad\qquad 3.8$$

Where, θ = temperature field $\left(\theta = \frac{\hat{\theta}-\hat{\theta}_{cold}}{\hat{\theta}_{hot}-\hat{\theta}_{cold}}\right)$, t = time, u = velocity, ∇ = vector gradient operator (grad), Re = Reynolds number, Pr = Prandtl number.

3.3   SIMULATION MODEL

In this study, OpenFoam software is used. The output is displayed using ParaView. The software caters a wide range of simulation such as the laminar flow that is used in this study. The incompressible flow of the fluid is chosen and a tutorial OpenFOAM folder 'icoFoam' is used. The geometry is modelled and meshed using a meshing software (Gmsh), and names are given for the surfaces. The mesh file is then converted to polymesh in OpenFoam to be accessible.

3.3.1 Analysis

Prior to running the simulation, the analysis is configured to be dimensionless, meaning that the quantity is projected as a pure number without the use of any physical units. Like the Reynolds number and Strouhal number, the number is typically defined as a ratio or product of quantities that do have units in a way that all the units cancel out.

3.3.2 Geometry design

Two setups are required which are one circular cylinder setup and two circular cylinder setup (Figure 3.2). The difference between each setup would be the presence of the downstream cylinder.
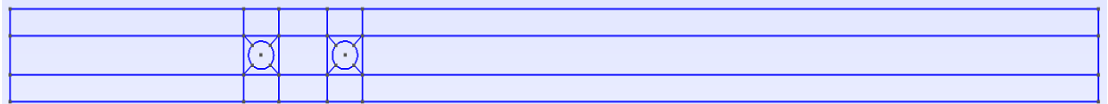
Figure 3.2 Geometry design for one circular cylinder setup made in Gmsh.

3.3.3 Meshing

The mesh used in Figure 3.3 is structured mesh and the region at the cylinder's edge has an increased meshed sizing to improve the solution's precision. The conditions

are set up and modified using Gmsh. Meshing is important because good mesh resulted in reducing the amount of time and effort spent to get accurate results.
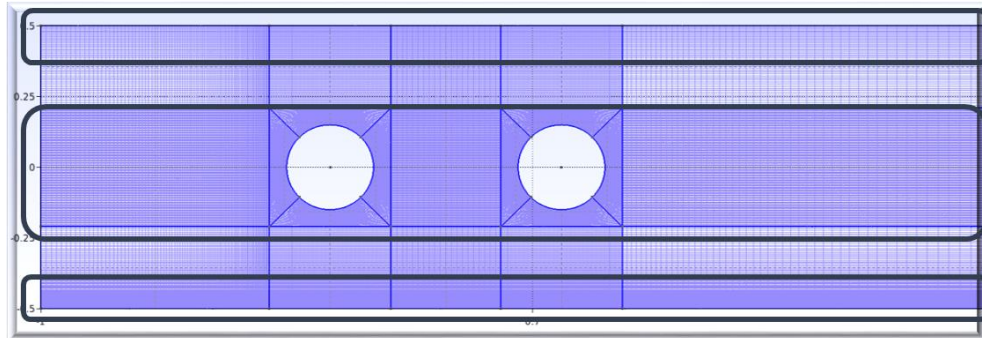
Figure 3.3 Mesh structure of the model.

3.3.4 Setting up parameters

i. Reynolds Number

The Reynolds Number cannot be set in OpenFoam. Thus, the value of the velocity at the inlet, and the height of the channel are used to obtain the desired Reynolds Number.

ii. Characteristic Length

The characteristic length that is used in this study is the inlet height, H.

iii. Diameter of Cylinder

The diameter of the cylinder, d is varied, meanwhile, the height of the channel, h is let to be constant which is $h=2$.

iv. Blockage Ratio, β

Blockage ratio is the ratio of diameter and height (d/h) will be set to constant for the experiment, $\beta=0.3$.

v. Gap Ratio (*G/h*)

The ratio of gap length (*G*) and the height (*h*) is set as a variable to be studied. The gap ratio would be in range of *G/h* = [1-2.4].

vi. Temperature Field, θ

The temperature of the bottom wall is θ = hot, and the top wall is θ = 0.

vii. Condition set up

The fully developed velocity profile is imposed at the inlet of the channel. The Kinematic Viscosity, *v*, varies according to the Reynolds number. The value of velocity, *u*, characteristic length (which is inlet height), *h*, and kinematic viscosity, *v,* is dependent on Reynolds Number (Equation 3.9).

$$Re = \frac{\rho V L}{\mu} = \frac{u L}{v} \qquad 3.9$$

Applying the no-slip boundary conditions at the top and bottom wall on Equation 3.7 produces the Hartmann profile, a fully developed quasi-two-dimensional flow (Poth'erat 2007), as presented below

$$u_x(y) = \frac{cosh\sqrt{H}}{cosh\sqrt{H} - 1}\left(1 - \frac{cosh\left(\sqrt{H}y\right)}{cosh\sqrt{H}}\right) \qquad 3.10$$

At zero Hartmann friction term, *H,* which in the limit H→0, the above equation 3.10 will present the Poiseuille profile of two-dimensional flow. In the occasion of a non-zero *H,* it tends to give almost a flat profile that is more prominent in a higher Hartmann friction term, *H.* The Lorentz force, which operates in the opposite direction of the flow, is influenced by the strength of the spanwise magnetic field, or *H,* in this present work (Barleon et al. 1996). The core region part of the fluid will flow with a higher velocity

when a no-slip condition is applied at the walls, which interacts with the magnetic field and generates more electric current than it does in the vicinity of the walls. The Lorentz force produced by the interaction of the magnetic field and the current will be greater when the electric current density is higher. This leads to the core region having a stronger Lorentz force that gives features of the near-flat profile in that region.

The Strouhal Number can be calculated by using the frequency of Vortex shedding (Equation 3.11) where f is the frequency of shedding, h is the characteristic length which is the height of the channel, and U is the inlet velocity.

$$St = \frac{fh}{u} \qquad\qquad 3.11$$

To proceed with the analysis of the result, the force library in the OpenFOAM is used to include the lift coefficient with respect to time in the post-processing result (Refer to Equation 3.12).

$$C_L = \frac{F_L}{\frac{1}{2}\rho u^2 h} \qquad\qquad 3.12$$

Where, F_L = lift force, ρ = fluid Density, u = fluid Velocity, h = reference Length (Inlet Height).

The local Nusselt number along the channel's bottom heated wall is defined as

$$Nu_w(x,t) = \frac{1}{\theta_f - \theta_w}\frac{\partial\theta}{\partial y}\bigg|_{wall} \qquad\qquad 3.13$$

Nu_w is the local Nusselt number at the trail of the heated side wall, and θ_f is the bulk fluid temperature. This value is computed using the velocity and temperature distribution along the stream as

$$\theta_f(x,t) = \frac{\int_0^h u\theta dy}{\int_0^h u\, dy} \qquad\qquad 3.14$$

Through the heated wall of the channel, the time-averaged Nusselt number for heat transfer is enumerated by considering the mean of the average local Nusselt number at different time step.

3.3.5 OpenFOAM simulation

The contour in Figure 3.4 below is the velocity contour that is done with OpenFoam and viewed in ParaView. The domain used is 2 in height and 50 in length. The flow started to become unsteady after passing by the cylindrical bluff body that acts as a vortex promoter.
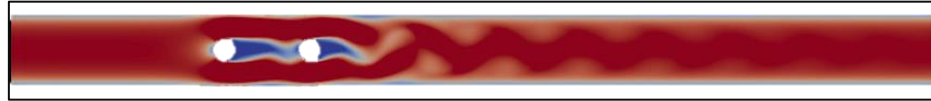
Figure 3.4 *x*-velocity contour done using OpenFOAM and viewed in ParaView

3.4   ONE CIRCULAR CYLINDER SETUP

The first case that will use this setup is for the validations in Chapter 4.2.1. The result validation is done for a bounded flow (similar to the two circular cylinder case experiments) with blockage ratio of 0.1, 0.2, and 0.3. A rectilinear plane channel with separated by a distance, *h*, contains a circular cylinder of diameter, *d* (Refer to Figure 3.5). Consider an incompressible fluid flowing inside the channel at a constant average velocity of *u*, with density ρ and kinematic viscosity *v*. The problem is governed by a dimensionless parameter: the channel Reynolds number $Re = uh/v$, and a geometrical parameter, which is the blockage ratio $\beta = d/h$.

The second case that will use this setup is to compare the result for flow past two circular cylinders and flow past one circular cylinder. The comparison is discussed in Chapter 4.3, 4.4 and 4.5. The blockage ratio, β, is set constant to be 0.3.
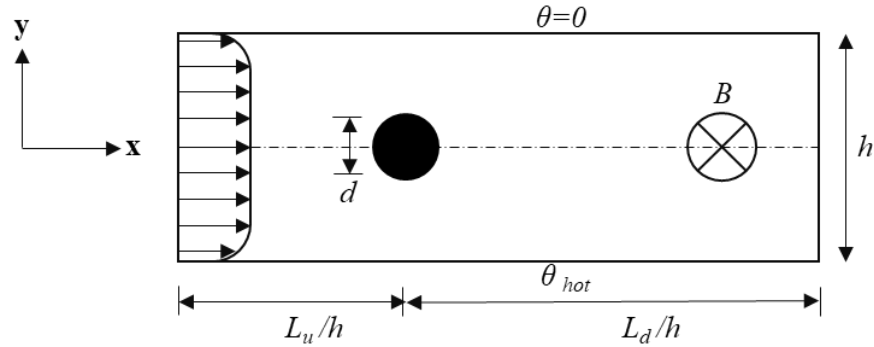
Figure 3.5 Schematic diagram of the computational domain for one circular cylinder case set up. The arrow represents the direction flow. The magnetic field, B, is parallel to the cylinder axis and acts in a z-direction which is in the out-of-plane direction

3.5   TWO CIRCULAR CYLINDER SETUP

The geometry design setup for two circular cylinder cases is as Figure 3.6. In this case, the blockage ratio will be constant with the value of $\beta = 0.3$ for both cylinders. The height is kept constant at $h = 2$ while the gap length is varied at $G/h = 1$, 1.2, 1.4 and 1.6 to achieve an optimum result.
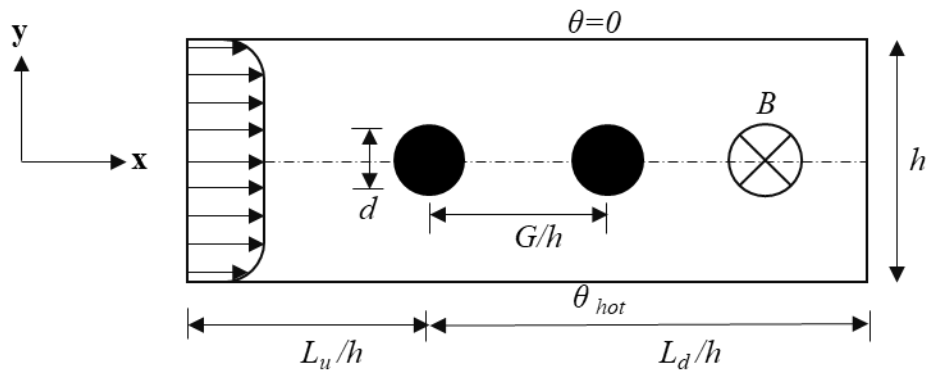
Figure 3.6 Two circular cylinder case set up. The arrow represents the direction of the flow.

23

In Figure 3.6, the height of the channel, L_u/h is the upstream length starting from the inlet to the centre of the upstream cylinder, L_d/h is the downstream length, and the diameter of the cylinder, respectively. The gap ratio between the cylinders is defined as G/h and the blockage ratio is $\beta=(d/h)$. Magnetohydrodynamics flow inside the channel in Figure 3.6 is governed by Eq. 3.7 for a quasi-2D model.

3.6 DETERMINATION OF CRITICAL REYNOLDS NUMBER

Simulations are made at $Re = $ [1-2500], firstly at an interval of 500, narrow down to 200, then 100. From there, the graphs of lift coefficient against time, as an example in Figure 3.7, are plotted, and the saturation of the graph is observed. The simulations to determine the critical Reynolds number are narrowed down based on plotting graphs. When there is a wake flow, it will result in positive and negative lift forces of periodic shift experienced by the cylinder as opposed to a steady flow that is indicated by the zero-lift coefficient. (Hamid & Noh, 2019). As seen in Figure 3.7 (a), (b), and (c), the figures show that the lift coefficient is still approaching zero. As the flow transition from Figure 3.7 (c) $Re = 560$ to Figure 3.10 (d) $Re = 570$, the C_L graph for $Re = 570$ is plotted with the appearance of fluctuation in the C_L value, which indicates that the flow is unsteady due to the presence of the cylinders that acts as bluff body inside the channel hence causing positive and negative lift forces. This means that between the range of $Re = $ [560-570], the flow starts to become unsteady, and the point where the flow is at the onset of unsteadiness lies between the range. Hence, the middle point between the range is taken as the Re_c value, which is $Re_c = 565$. In Figure 3.7 (e), the fluctuation of the C_L in the graph is already constant at a stable value of $C_L = 0.034$.
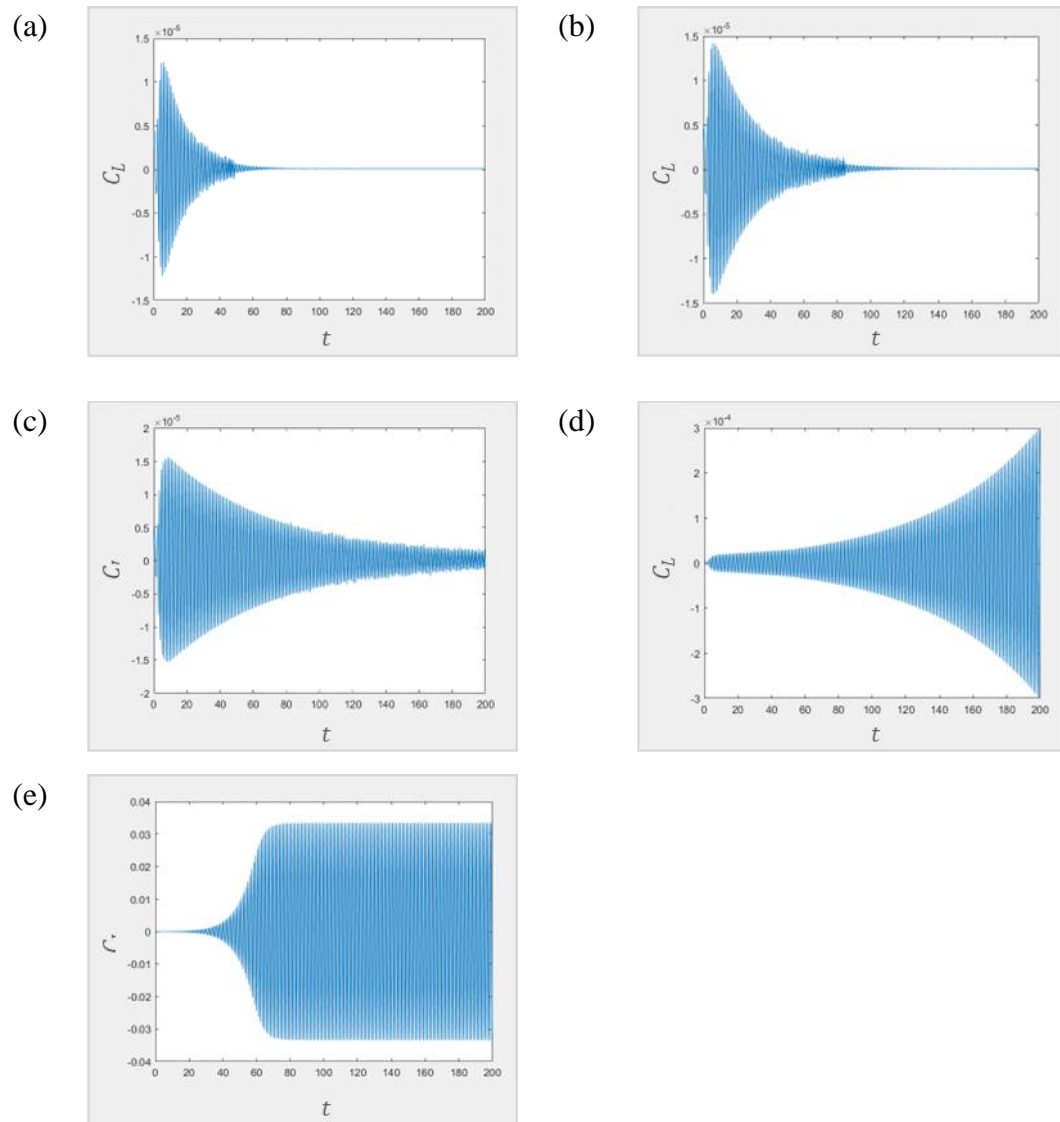
(a)

(b)

(c)

(d)

(e)

Figure 3.7 The graph of lift coefficient plotted against time for (a) $Re = 540$, (b) $Re = $
550, (c) $Re = 560$, (d) $Re = 570$, (e) $Re = 620$ at $H = 200$ and $G/h = 1.2$.

CHAPTER FOUR

RESULTS

4.1 MESH AND DOMAIN DEPENDENCY STUDY

The dependency study is made based on the percentage of error for lift coefficient and Strouhal number, where these two terms are important when analyzing unsteady and oscillating flow problems.

4.1.1 Mesh Dependency Study

The data tabulated in Table 4.1 shows that at mesh M_4, the percentage of error for the Strouhal number starts to become constant. Increasing the number of elements beyond mesh M_4 does not show any significant improvement in the Strouhal number of the flow. Hence, M_4 is used after this onwards in this study,

Table 4.1 Percentage of error for Strouhal number
calculated with different nodes multiplier of 0.6, 0.7,
0.8, 1, 1.2, 1.4, 1.5.

Mesh	Nodes Multiplier	No. of Elements	St	Error, St (%)
M_1	0.6	20876	0.91743	**2.11**
M_2	0.7	26798	0.89847	**0.27**
M_3	0.8	35096	0.89606	**0.36**
M_4	1.0	52916	0.89286	**0.09**
M_5	1.2	74336	0.89366	**0.09**
M_6	1.4	99356	0.89286	**0.18**
M_7	1.5	111718	0.89445	

4.1.2   Domain Dependency Study

In this study, the upstream length is crucial to ensure that the flow is fully developed once it enters the cylinder. Based on Table 4.2, and Figure 4.1 the domain length does not pose any notable enhancement on the result. Thus, the upstream length, $L_u/h = 3$ is chosen ($8d$) in reference to Hussam and Sheard (2013).

Table 4.2 Percentage of error for Strouhal number and Lift coefficient at upstream, L_u = 1, 2, 3, 4, 5, 6 and 7.

Length	Cl	Error, Cl (%)
1	0.0021642	**0.70%**
2	0.0021794	**0.01%**
3	0.0021797	**0.01%**
4	0.0021799	**0.01%**
5	0.0021800	**0.01%**
6	0.0021798	**0.03%**
7	0.0021791	**0.16%**

(a) $L_u = 1$

(b) $L_u = 2$

(c) $L_u = 3$

(d) $L_u = 4$

(e) $L_u = 5$
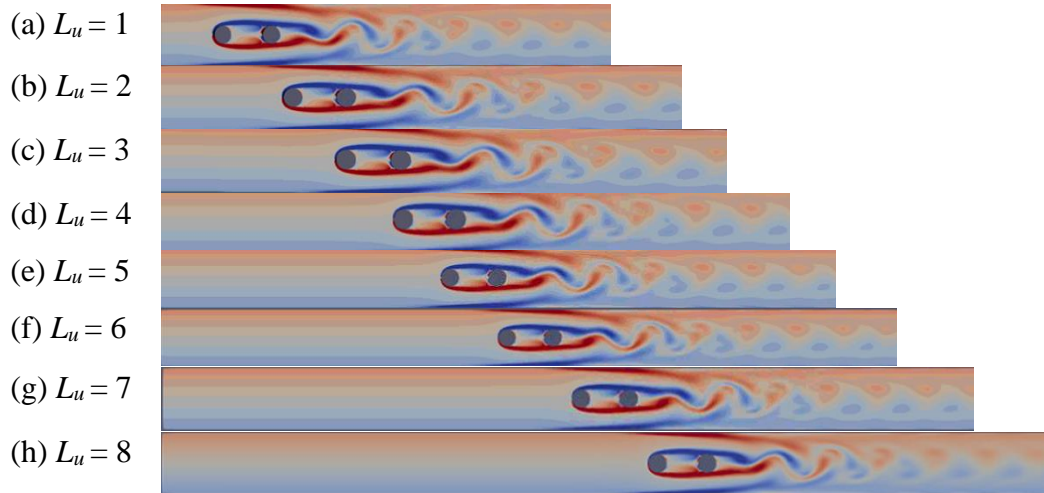
(f) $L_u = 6$

(g) $L_u = 7$

(h) $L_u = 8$

Figure 4.1 Vorticity contour captured at upstream length, L_u = (a) 1, (b) 2, (c) 3, (d) 4, (e) 5, (f) 6, (g) 7 and (h) 8 for hydrodanymics case at $Re = 1000$.

4.2 VALIDATIONS

4.2.1 Validation Of The Numerical System For Hydrodynamics.

Validation is made against published results to ensure the accuracy of the present formulation and model. The first test concerns critical Reynolds number (Re_c), which represents the threshold of Reynolds number where the flow changes from steady to unsteady flow, in a zero Hartmann flow without the effect of the magnetic field. The test is made with regards to the blockage ratio, β of 0.1, 0.2 and 0.3, whereby the critical Reynolds number is investigated. The results obtained are compared with the published numerical results of Chen et al. (1995), Sahin and Owen (2004) and Hussam et al. (2011). From the three points that have been validated (i.e. β = 0.1, 0.2, 0.3), a close agreement between the present data and published data is observed (refer Figure 4.2).
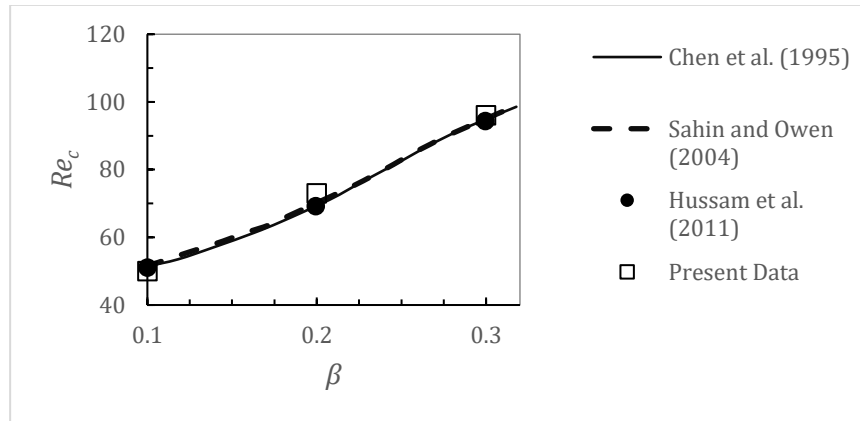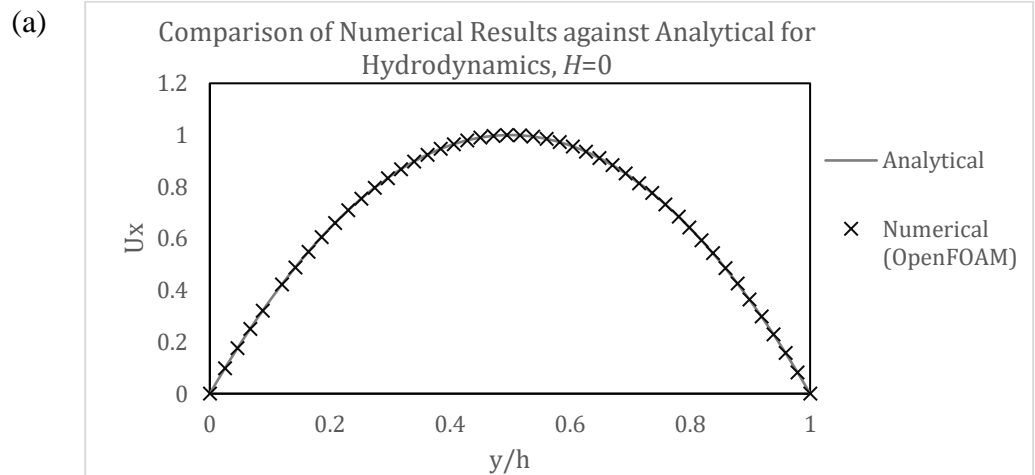

Figure 4.2 A graph of critical Reynolds number, Re_c against blockage ratio, β. Hollow symbols represent present data, while bullets, solid lines and dashed lines show data published in Hussam et al. (2011), Chen et al. (1995), Sahin and Owen (2004) respectively.

4.2.2 Validation of analytical and numerical results for MHD solver in OpenFOAM.

This present study is done using an MHD solver in OpenFOAM. To validate the result of the solver, the analytical solution (Equation 3.10) is compared with MHD OpenFOAM for the fully developed velocity profile at the inlet. The simulation is tested in an empty channel.

In Figure 4.3, the comparison of the numerical results and the analytical solution (Equation 3.10) is presented. The velocity profile at the inlet and outlet for a hydrodynamics case and for MHD cases (H = 50, 100 and 200), are plotted, and the curve for all the results agrees well at maximum velocity, U_{max} = 1. This study shows that the fully developed velocity profile solution in OpenFOAM is successful.

Based on Figure 4.3, at H = 0, the curve can be observed to be a parabolic profile, and as H increases, the profile becomes fuller and flattened towards a "top-hat" profile (Hussam et al., 2011). The inlet and outlet velocity of the channel seems to be in good agreement.

(a)

(b)

Comparison of Numerical Results against Analytical for *H*=50

(c)

Comparison of Numerical Results against Analytical for *H*=100

(d)

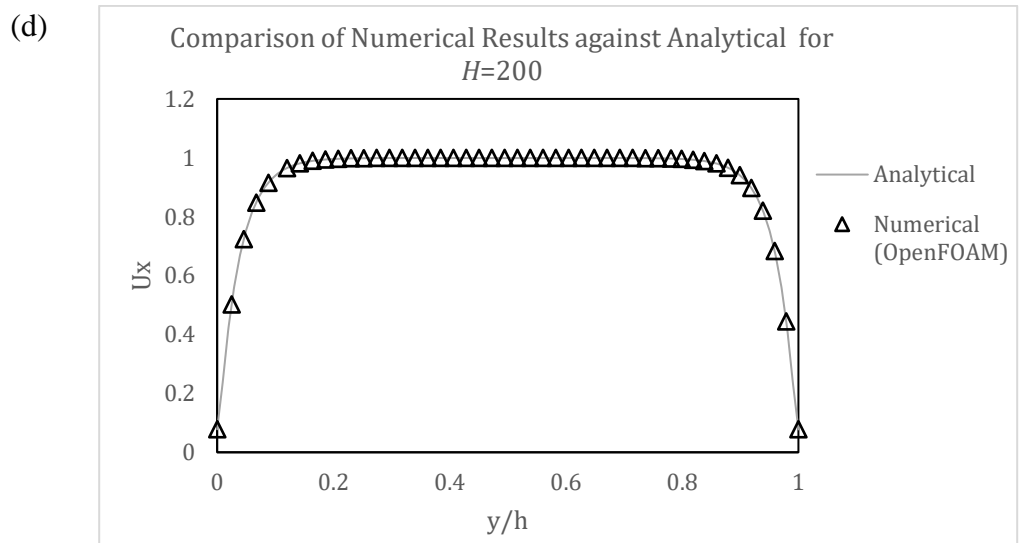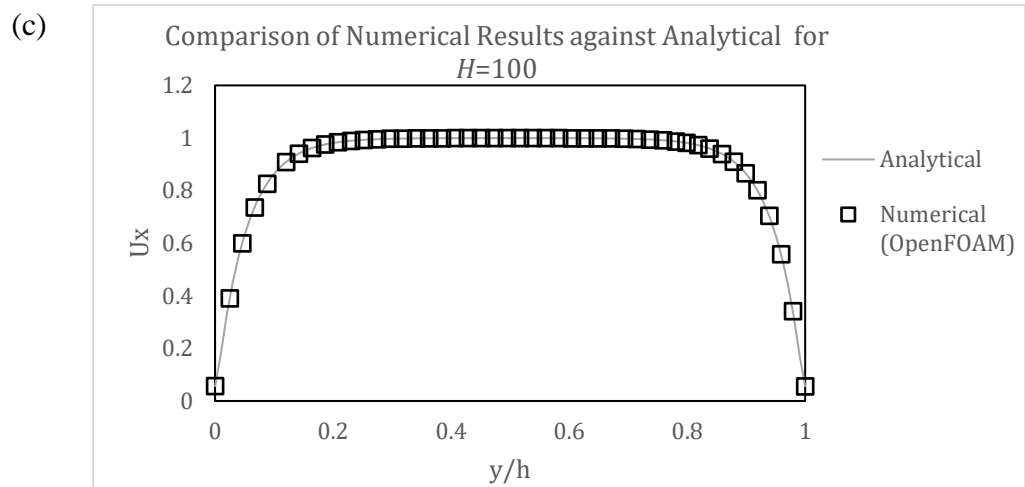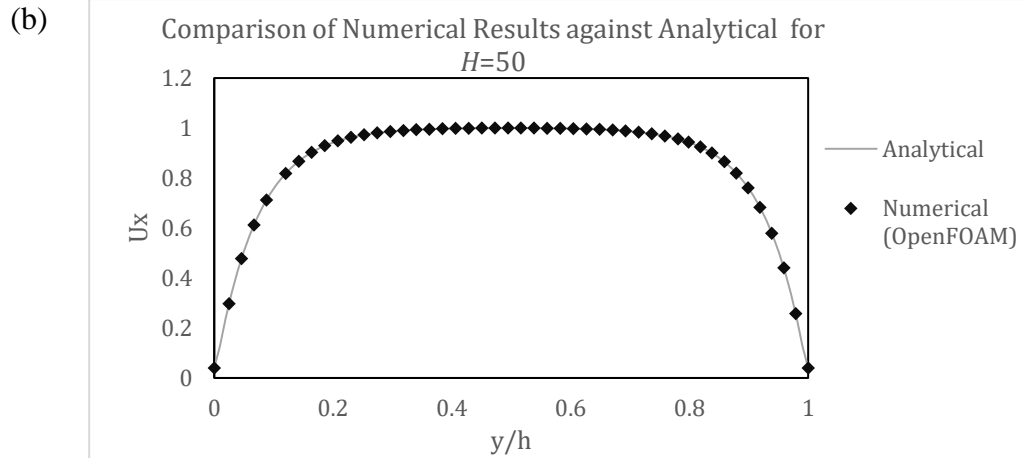Comparison of Numerical Results against Analytical for *H*=200

Figure 4.3 The streamwise velocity profile of OpenFOAM results against theoretical solutions for (a) *H*=0, (b) *H*=50, (c) *H*=100, and (d) *H*=200.

4.3 EFFECT OF GAP RATIO AND HARTMANN PARAMETER ON CRITICAL REYNOLDS NUMBER.

In order to achieve and satisfy the objectives of this project, simulations are made to illustrate the changes between HD and MHD flow. The effect of the Hartmann parameter on Rec is discussed, followed by the dependency of the critical Reynolds number on the gap ratio (G/h).

4.3.1 Hydrodynamics and Magnetohydrodynamics

To perceive a better understanding on the effect of MHD on flow structure, vorticity contour at G/h = 1.2 and Re = 400 for HD flow (H = 0) and MHD flow (H= 200) are presented in Figure 4.4.
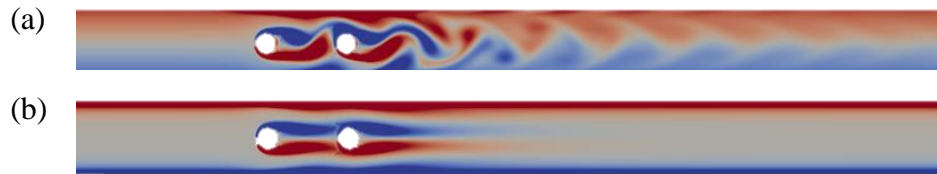
Figure 4.4 The z-vorticity contour captured for (a) hydrodynamics (H = 0), and (b) magnetohydrodynamics flow (H = 200) to illustrate the difference in flow regime at gap ratio, G/h = 1.2, Re = 400.

As shown in Figure 4.4, the flow regime in the case of HD has vorticity, whereby MHD does not has a counterpart like in the case of purely HD flow. This regime, as such in HD is to confine cylinder wakes in particular, where the side walls' boundary layers are likely to separate, promoting vortex shedding (Farahi & Hossein, 2017). As the wake advection moves downstream, the wake vortices from the downstream cylinder are seen to be stretched out. According to Verma and Govardhan (2011), separation occurs when fluid flows over a body where it is causing period shedding of vortices to occur for the flow. At the same Reynolds number, the HD flow becomes unsteady, while the MHD flow is not yet to be at the onset of unsteadiness.

4.3.2 Effect of Hartmann parameter on critical Reynolds number

For MHD flow to have such vorticity induced, flow with a higher Reynolds number must be introduced to the channel, as seen in Figure 4.5. In the figure, the vorticity contour displayed is for $G/h = 1.2$, with $Re = 1500$ at lower H of 200 and higher H of 600. At $H = 200$, the flow managed to induce Karman vortice. As the Hartmann parameter is increased further ($H = 600$), the vortex shedding is completely suppressed, where the flow becomes a steady flow. The shear layer observed at the upstream cylinder starts to converge and no longer creates attachment with the downstream cylinder.
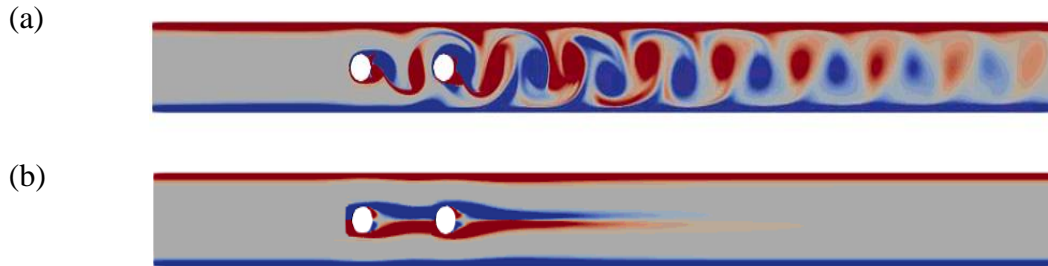
(a)

(b)

Figure 4.5 The z-vorticity contour captured for gap ratio, $G/h = 1.2$, $Re = 1500$ at Hartmann parameter (a) $H = 200$ and (b) $H = 600$.

The graph in Figure 4.6 demonstrates the effect of the Hartmann parameter on the critical Reynolds number. As the Hartmann parameter increases from $H = 0$ to $H = 200$, the critical Reynolds number increases for all the gap ratios, $G/h = [1-2.4]$. This is due to the suppresion of instability in the flow structure by the Lorentz force presence in an MHD flow that acts like a damping force. It is experimentally established that the application of an external magnetic field can suppress two-dimensional instabilities (Chatterjee et al., 2013). From the same graph (Figure 4.6), it is noticeable that the critical Reynolds number is highest at $G/h = 1$ and started to decrease in value towards $G/h = 1.2$. the Re_c at $G/h = 1.2$. would be the peak value for the lowest Re_c because the gap ratio, after that, started to increase and later had an almost constant value of onset unsteadiness.
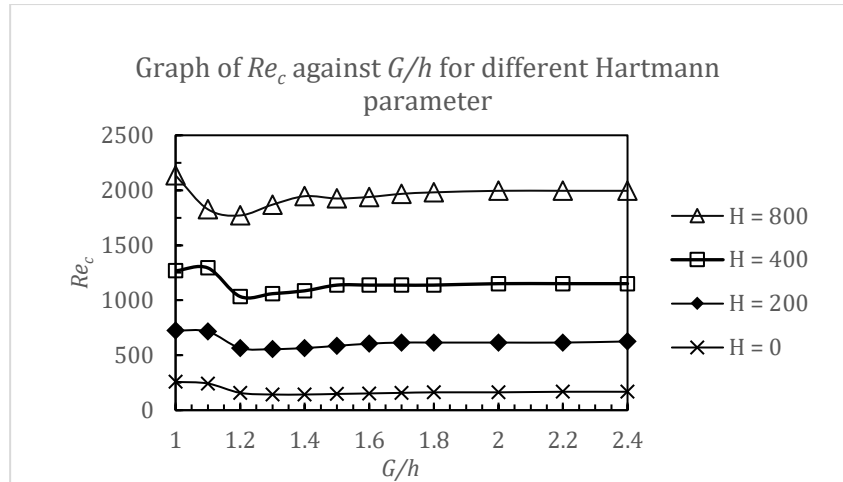
Figure 4.6 Graph of critical Reynolds number, Re$_c$ plotted against gap ratio, *G/h* at different Hartmann parameters (*H* = 0, *H* = 200, *H* = 400, *H* = 800).

4.3.3 Effect of Gap Ratio on critical Reynolds number

To illustrate the effect of *G/h* on the flow, Figure 4.7 is presented with different *G/h* and also for a single cylinder. Figure 4.7 is indicative of multiple bluff body attributes that have a significant impact on the flow as compared to a single circular bluff body. The boundary layer detachment and the entrainment of the boundary layer from the walls on account of the vortex shedding from the cylinder occurs downstream of the cylinder, where it is only observed at *G/h* = 1.2, 1.4 and 1.6. The downstream cylinder is fully engulfed in the wake developed from the upstream cylinder causing the vortex resulting from the upstream cylinder to amplify (Assi & G.R, 2014). The observation agrees well with the finding of Hussam and Sheard (2011). The same incident cannot be seen in the flow with *G/h* = 1 and with a single cylinder in which the flow shows no vortex shedding in both cases.
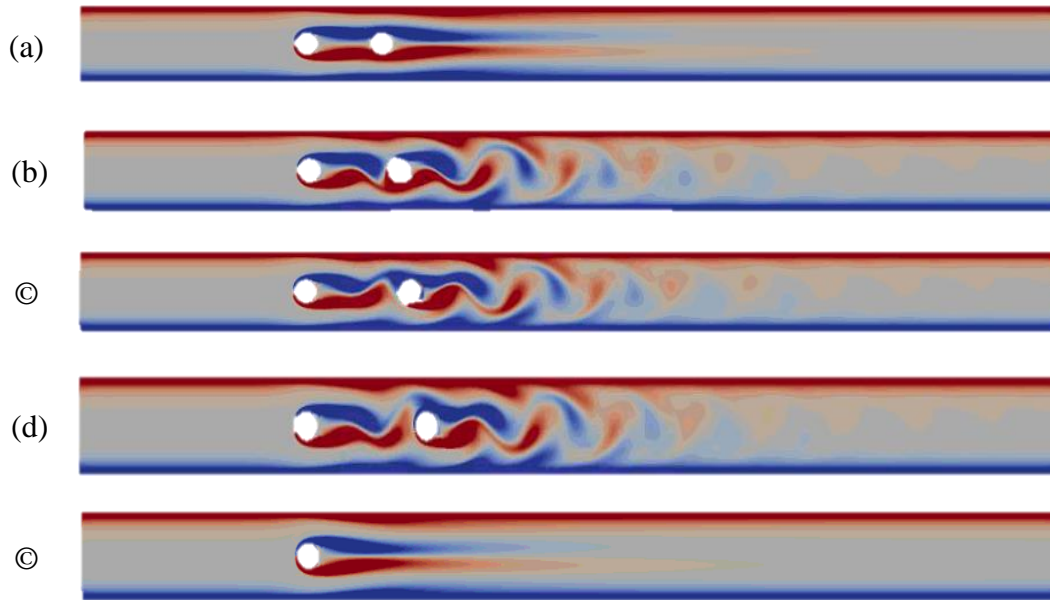
(a)

(b)

©

(d)

©

Figure 4.7 The z-vorticity contours for *G/h*=(a) 1, (b) 1.2, (c) 1.4, (d) 1.6 and for ©
single cylinder at *Re* = 600 and *H* = 200.

Unsteady flow is managed to be achieved for *G/h* = 1.2, 1.4 and 1.6, in the case of having Reynolds number due at the onset of unsteadiness being lower than that of the single cylinder. This can be further exemplified by the graph presented in Figure 4.8. The Reynolds number at the onset of steadiness for the case of *G/h* = 1 is seen to be higher than the case of a single cylinder, and this does not suit the purpose of placing two circular cylinder bluff bodies in the channel to promote vortex shedding and unsteadiness in the flow.

Proceeding *G/h* = 1.6, at *G/h* = 1.8, 2 and 2.2, in Figure 4.8 (a) (b), the *Re$_c$* is the same as *Re$_c$* for a single cylinder, showing that they act as single cylinder. This means that at *G/h* = 1.8, 2, and 2.2, the upstream and downstream cylinders started to act like a single bluff body, each their own. The detachment of the vortex shedding no longer occurs and the two bluff bodies do not seem to amplify the vortex shedding anymore. Whereas, in Figure 4.8 (c), *G/h* = 1.8, 2, and 2.2, the *Re$_c$* value is higher than the benchmark single cylinder, which may result from the braking force of Hartmann friction term.
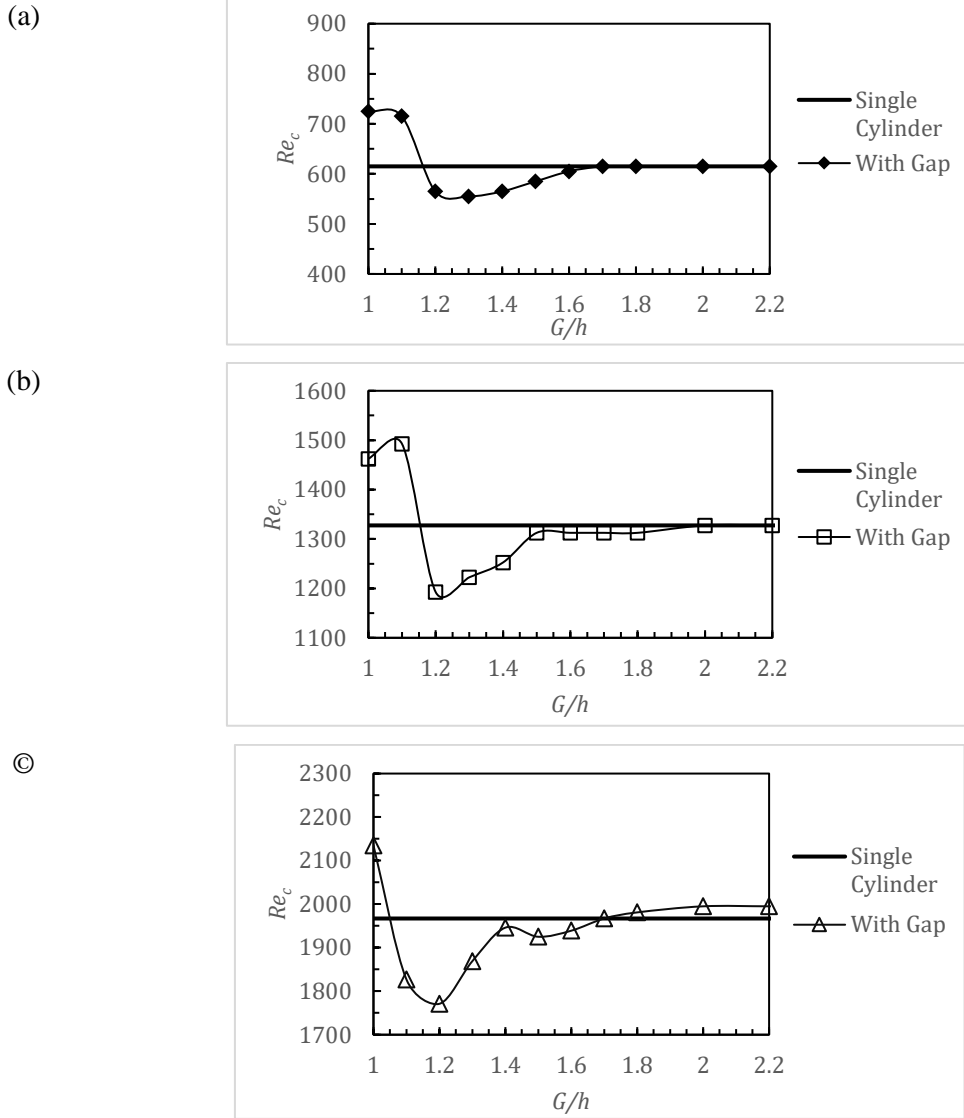
35

(a)

(b)

©

Figure 4.8 The comparison of critical Reynolds number for flow pass single cylinder and two cylinders with (a) $H = 200$, (b) 400, and (c) 800, respectively.

4.4 EFFECT OF GAP RATIO AND HARTMANN PARAMETER ON PRESSURE DROP

4.4.1 Effect of Gap Ratio on Pressure drop

The addition of the downstream cylinder inside the channel would lead to an increase in pressure drop. Thus, it is keen to study the effect of adding the downstream cylinder and the effect of gap length on the pressure drop. Due to that, the additional pressure drop penalty of adding the downstream cylinder is considered. Pressure drop penalty means the value of the pressure drop is the calculated difference with flow pass single cylinder for each cases. In Figure 4.9, the pressure drop penalty is plotted against Re. The baseline pressure drop would be that of a single cylinder, and the pressure drop penalty would be calculated as the difference between the pressure drops of flows past two circular cylinders and flows past a single cylinder. The value is taken at the outlet of the channel. Based on the graph, it is demonstrated that at low H ($H = 200, 400$), the pressure drop for adding a downstream cylinder at $G/h = 1$ is the lowest compared to the rest of the cases, while the pressure drop increases with increasing gap ratio from $G/h = 1.2$ to $G/h = 1.6$. In contrast, the pressure drop penalty is very small at $H = 800$ between each gap ratio. This would make the pressure drop at low H to be dependent on the gap length between the cylinders when the cylinders' size is fixed at a constant diameter.

For Figure 4.9 (a), (b), (c), the pressure drop penalty from $Re = 200$ to $Re = 1200$ decreases due to the increasing Reynolds number that managed to overcome the Lorentz effect that acts in an opposite direction of the flow in the channel.
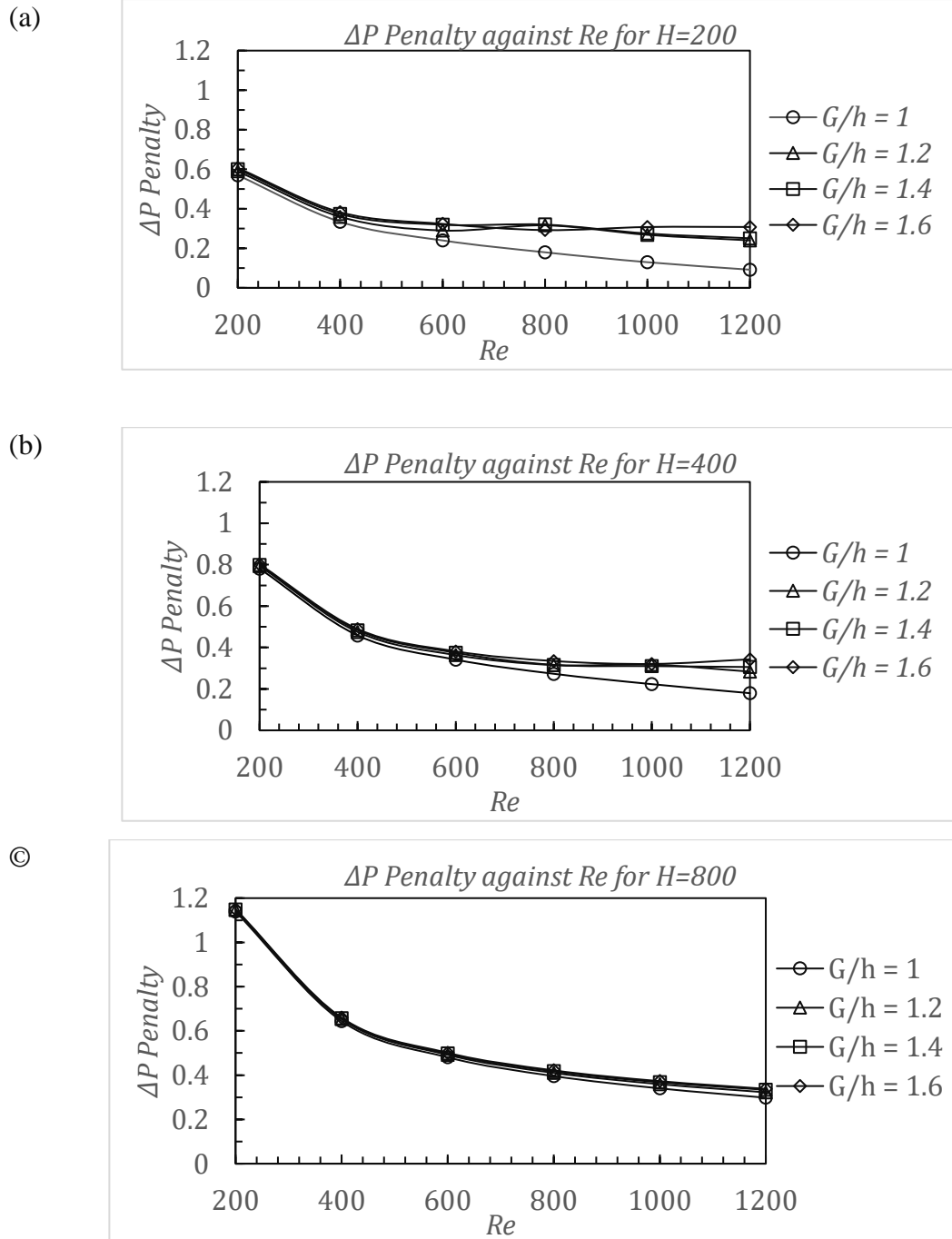
(a)

(b)

©

Figure 4.9 The pressure drop penalty against Reynolds number for the flow at *H* = (a) 200, (b) 400, and (c) 800, at *G/h* = 1, 1.2, 1.4 and 1.6.

4.4.2 Effect of Hartmann parameter on Pressure drop

In the case of MHD channel flow, a high Hartmann parameter causes a significant pressure drop (Hussam & Sheard, 2011), and this agrees well with the results that have been obtained. Figure 4.10 shows that as the Hartmann parameter increases from $H = 200$ to $H = 800$, the pressure drop penalty increases across the channel for all the cases. This is because the Lorentz forces produced have a substantial impact on the pressure field (Rhodes et al., 2018) as the forces produced are in the direction opposing to the flow, which causes the significant value in pressure drop. At $H = 800$, the difference in pressure drop penalty for each gap ratio no longer possess large difference like in H=200 and H=400.
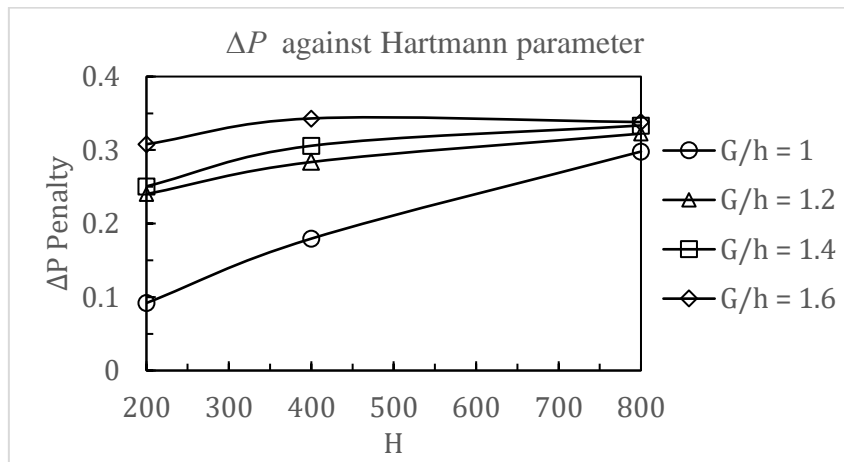

Figure 4.10 The pressure drop penalty is plotted against H at G/h = 1, 1.2, 1.4 and 1.6, and Re = 2400.

4.5 EFFECT OF GAP RATIO AND HARTMANN PARAMETER ON HEAT TRANSFER EFFICIENCY

The heat transfer efficiency due to the effect of gap length and Hartmann parameter is discussed in terms of Nusselt number.
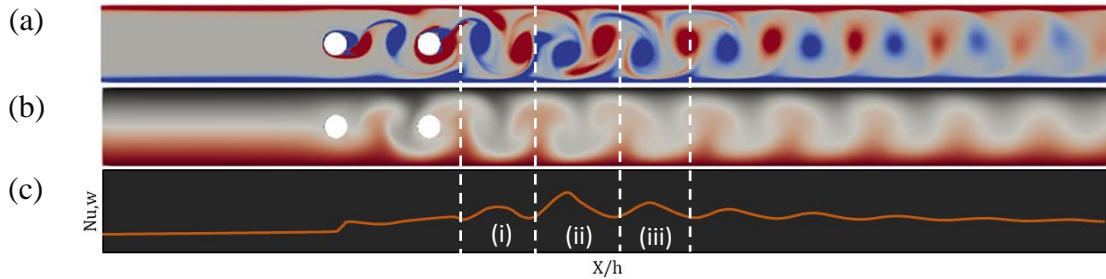

Figure 4.11 Contour for flow at $H = 200$, $G/h = 1.2$, $Re = 2000$ (a) Vorticity contour, (b) Temperature contour and (c) Local Nusselt number at x-locations along the length of the channel.

Based on Figure 4.11 I (i), (ii), (iii), the temperature gradient after the downstream cylinder gives a significant fluctuation which shows that heat is transferred faster at unsteady flow. It causes a higher heat transfer drive which leads to a higher Nusselt number. The temperature gradient is calculated for a point, y, that is very near to the heated side wall. The temperature gradient before the upstream cylinder is -0.04 while the temperature gradient after the downstream cylinder is -0.07, where the negative value is due to temperature at the point, y being lesser than of the heated wall. The higher temperature gradient value after the downstream cylinder strengthens the illustration in Figure 4.11(b), whereby after the upstream cylinder, the temperature contour is seen to be fluctuating.

4.5.1 Effect of Gap Ratio on Nusselt number

A graph of time-averaged Nusselt number as a function of Reynolds number for gap ratio, $G/h = 1$, 1.2, 1.4 and 1.6, for $H = 400$ is plotted and presented in Figure 4.12. As

seen in the figure, at gap ratio, $G/h = 1$, the Nusselt number is lower than those of the single cylinder. This gap ratio ($G/h = 1$) does not optimize the flow in terms of heat transfer. At gap ratio, $G/h = 1.2$, 1.4 and 1.6, there is an exceptional change in Nu as compared to flow past a single cylinder and flow past two cylinders with gap ratio, $G/h = 1$. There is a slight decrease in Nu for $G/h = 1.2$, 1.4 as compared to $G/h = 1.6$. Apart from all that, at $G/h = 1.2$, 1.4 and 1.6 Nu is found to be improved by imposing the two circular cylinders at these gap ratio. This is because, at the right gap ratio, the shedding of the flow will increase. When this happens, the flow becomes unsteady at a lower Re, and this promotes heat transfer inside the channel of the flow. Since, the Re_c results for $G/h = 1$ is higher than $G/h = 1.2$, 1.4, 1,6, the convection also tends to be slower.
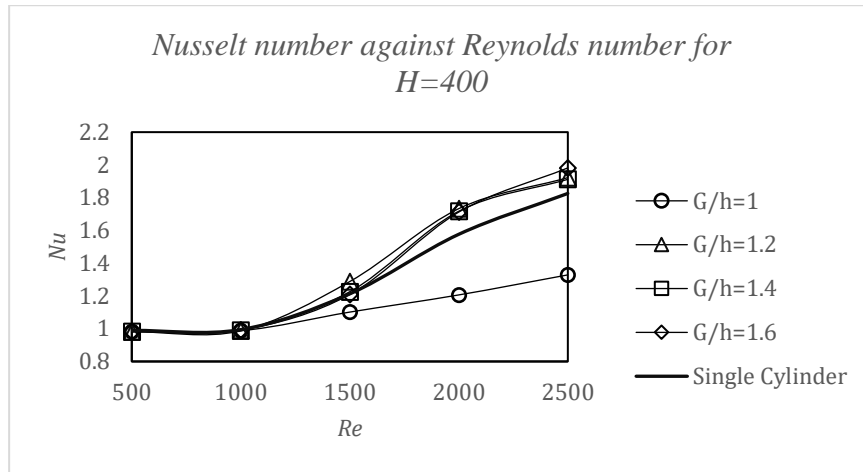
Figure 4.12 Time-averaged Nusselt number shown as a function of Reynolds number for a single cylinder and two circular cylinders with $G/h=1$, 1.2, 1.4 and 1.6 at $H=400$.

4.5.2 Effect of Hartmann parameter on Nusselt number

For this discussion, $G/h = 1$ and $G/h = 1.2$ are chosen to illustrate the difference in Nu. Since $G/h = 1.2$ is found to have an exceptional result in terms of Critical Reynolds number, the Nu result for $G/h = 1.2$ is used as a comparison with $G/h = 1$, which has the highest critical Reynolds number among the results for other gap ratios. Figure 4.13 shows the effect of the Hartmann parameter on the time-averaged Nusselt number for $G/h = 1$ and 1.2. After the flow reaches the critical Re, the flow shows a notable increase

in *Nu* due to the unsteady state of the flow regime. From the two graphs, it can be seen that there is a spike in Nu for *G/h* = 1.2 as compared to *G/h* = 1. Overall, a conclusion that can be made from Figure 4.13 is that a higher Hartmann parameter will result in a lower Nusselt number, and this relationship is dependent on the gap ratio, *G/h*.

(a)
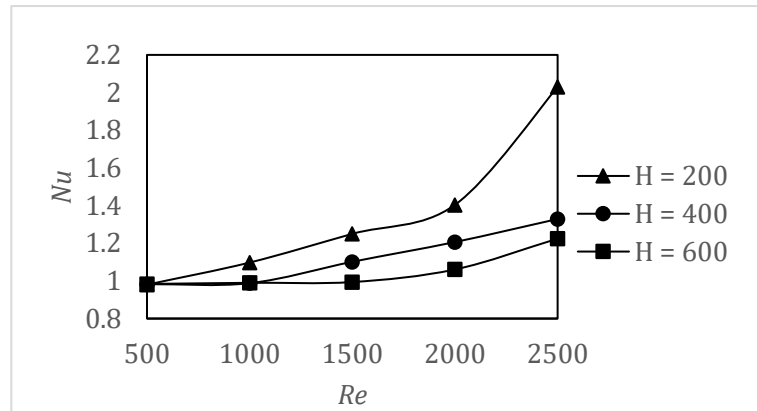
(b)
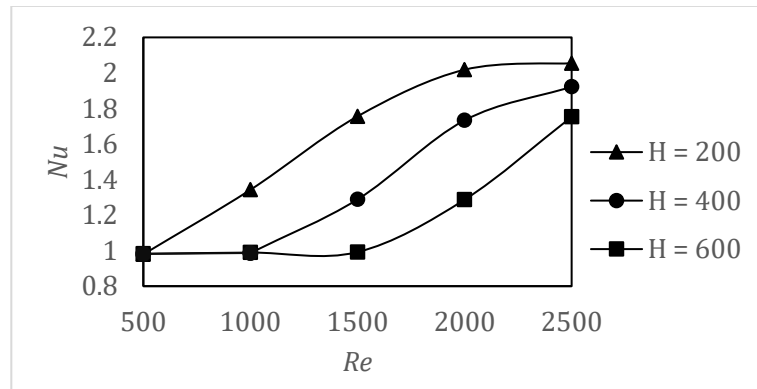

Figure 4.13 Time-averaged Nusselt number shown as a function of Reynolds number at *H* = 200, 400, 600 for (a*)* *G/h* = 1 and (b) *G/h* = 1.2.

CHAPTER FIVE

CONCLUSION

5.1 CONLUSION

This study is investigated numerically on the structure of liquid metal flow and heat transfer past a circular cylinder bluff body in a rectangular duct when it is comprehended to a magnetohydrodynamics effect. Under these conditions, the flow is quasi-two-dimensional. This study is solved in a two-dimensional domain, by using the modified Navier-Stokes equations.

In this study, the effect of gap ratio, G/h = 1, 1.2, 1.4 and 1.6 and Hartmann parameter = [0-800] are analyzed for the critical Reynolds number, pressure drop and Nusselt number. Gap ratio, G/h = 1.2, 1.4 and 1.6 are discovered to be improving flow's critical Reynolds number of the flow to a lower value as compared to flow past a single cylinder. While the critical Reynolds number at gap ratio, G/h = 1, is higher than the single cylinder even though the pressure drop penalty is lowest compared to the rest of the gap ratio. Gap ratio, G/h = 1 and 1.2 are then analyzed to determine the Nusselt number of the flow, and only G/h = 1.2 has an enhancement of Nusselt number as compared to the single cylinder while the flow with G/h = 1 has Nusselt number below the single cylinder. Increasing the Hartmann parameter from H = 200 to H = 600 resulted in an increase in critical Reynolds number, pressure drop and a decrease in Nusselt number. To conclude, flow past two cylinders at gap ratio, G/h = 1.2, 1.4 and 1.6 managed to create an unsteady flow with a critical Reynolds number of lesser than the single cylinder and with substantial increment on the Nusselt number, and when a higher Hartmann parameter is introduced, it will suppress the enriching effect of the flow gradually with additional in pressure drop penalty.

5.2 RECOMMENDATION FOR FUTURE RESEARCH

To boarden current studies, the effect of magnetic field on the flow behind two circular cylinder, it is keen to pursue the research while including continuous (more than two) bluff bodies in a tandem arrangement.

REFERENCES

Assi, G. R., Bearman, P. W., & Meneghini, J. R. (2010). On the wake-induced vibration of tandem circular cylinders: the vortex interaction excitation mechanism. *Journal of Fluid Mechanics*, *661*, 365-401.

Assi, G. R. (2014). Wake-induced vibration of tandem cylinders of different diameters. *Journal of Fluids and Structures*, *50*, 329-339.

Aylı, E., & Bayer, Ö. (2019). Optimization of Vortex Promoter Parameters to Enhance Heat Transfer Rate in Electronic Equipment. Journal of Thermal Science and Engineering Applications, 12(2).

Barleon, L., Mack, K. J., & Stieglitz, R. (1996). The MEKKA-facility: A flexible tool to investigate MHD-flow phenomena. Karlsruhe, Germany: Forschungszentrum Karlsruhe.

Ben Hadid, H., Henry, D., & Kaddeche, S. (1997). Numerical study of convection in the horizontal Bridgman configuration under the action of a constant magnetic field. Part 1. Two-dimensional flow. Journal of Fluid Mechanics, 333, 23-56. doi:10.1017/S0022112096004193

Branover, H. 1978 Magnetohydrodynamic flow in ducts. Halsted Press, New York, NY.

Cassells, O. G., Hussam, W. K., & Sheard, G. J. (2016). Heat transfer enhancement using rectangular vortex promoters in confined quasi-two-dimensional magnetohydrodynamic flows. International Journal of Heat and Mass Transfer, 93, 186-199.

Cengel, Y. A., & Ghajar, A. (2015). Heat Transfer, Fundamentals and Application.

Chatterjee, D., Chatterjee, K., Mondal, B., & Hui, N. B. (2014). Wall-Confined Flow and Heat Transfer Around a Square Cylinder at Low Reynolds and Hartmann parameters. Heat Transfer—Asian Research, 43(5), 459-475.

Davidson, P. A. (2002). An introduction to magnetohydrodynamics. American Journal of Physics *70*(7), 781. https://doi.org/10.1119/1.1482065

DePuy, T. R. (2010). Fluid dynamics and heat transfer in a Hartmann Flow. *Rensselaer Polytechnic Institute, Master of Engineering in Mechanical Engineering Thesis*.

Dobran, F. (2012). Fusion energy conversion in magnetically confined plasma reactors. *Progress in Nuclear Energy*, *60*, 89-116.

Farahi, S. M., & Hossein, N. A. (2017). Investigation of magnetohydrodynamics flow and heat transfer in the presence of a confined square cylinder using SM82 equations. *Thermal Science*, *21*(2), 889-899.

Fiorentini, G., Ricci, B., & Villante, F. L. (2004). Nuclear fusion in the sun. Progress of Theoretical Physics Supplement, 154, 309-316.

Hamid, A.H.A., Hussam, W.K., Potherat, A. & Sheard, G.J (2015) Spatial evolution of a quasi-two-dimensional Karman vortex street subjected to a strong uniform magnetic field. Physics of Fluids **27** (5), 053602.

Hamid, A.H.A., Hussam, W.K., & Sheard, G.J. (2016) Combining an obstacle and electrically driven vortices to enhance heat transfer in a quasi-two-dimensional MHD duct flow. Journal of Fluid Mechanics **792**, 364-396.

Hamid, A. H. A., & Noh, M. H. M. (2019). Laminar Flows Over Equilateral Triangular Cylinders in Tandem Arrangement.

Hussam, W. K., Thompson, M. C. & Sheard, G. J. (2011). Dynamics and heat transfer in a quasi-two-dimensional MHD flow past a circular cylinder in a duct at high Hartmann parameter. International Journal of Heat and Mass Transfer **54** (5), 1091-1100.

Hussam, W. K., Thompson, M. C. & Sheard, G. J. (2012a) Enhancing heat transfer in a high Hartmann parameter magnetohydrodynamic channel flow via torsional oscillation of a cylindrical obstacle. Phys. Fluids 24 (11), 113601.

Hussam, W. K., Thompson, M. C. & Sheard, G. J. (2012b) Optimal transient disturbances behind a circular cylinder in a quasi two-dimensional magnetohydrodynamic duct flow. Physics of Fluids **24** (2), 024105.

Hussam, W. K., & Sheard, G. J. (2013). Heat transfer in a high Hartmann parameter MHD duct flow with a circular cylinder placed near the heated side-wall. International Journal of Heat and Mass Transfer, 67, 944-954.

Hussam, W. K., Hamid, A. H., Ng, Z. Y., & Sheard, G. J. (2018). Effect of vortex promoter shape on heat transfer in MHD duct flow with axial magnetic field. *International Journal of Thermal Sciences*, *134*, 453-464.

J.H. Chen, W.G. Pritchard, S.J. Tavener, Bifurcation for flow past a cylinder between parallel planes, J. Fluid Mech. 284 (1995) 23–41.

J. Moreau, R. Sommeria, Electrically driven vortices in a strong magnetic field, J. Fluid Mech. 189 (1988) 553–569.

J. Sommeria, R. Moreau, Why, how, and when, MHD turbulence becomes two dimensional, J.Fluid Mech. 118 (1982) 507–518.

J. A. Shercliff, The Theory of Electromagnetic Flow Measurement (Cambridge University Press, Cambridge, 1962).

Kreith, F., Manglik, R. M., & Bohn, M. S. (2012). *Principles of heat transfer*. Cengage learning.

M. Sahin, R.G. Owens, A numerical investigation of wall effects up to high blockage ratios on two-dimensional flow past a confined circular cylinder, Phys. Fluids 16 (2004) 1305–1320.

Malghan, V. R. (1996). History of MHD power plant development. Energy conversion and management, 37(5), 569-590.

Meis, M., Varas, F., Velázquez, A., & Vega, J. M. (2010). Heat transfer enhancement in micro-channels caused by vortex promoters. International Journal of Heat and Mass Transfer, 53(1–3), 29–40. https://doi.org/10.1016/j.ijheatmasstransfer.2009.10.013.

Mirnov, S. V. (2018). Tokamak evolution and view to future. *Nuclear Fusion*, *59*(1), 015001.

Mittal, S., & Kumar, V. (2001). Flow-induced oscillations of two cylinders in tandem and staggered arrangements. *Journal of Fluids and Structures*, *15*(5), 717-736.

Moffatt, H. (1967) On the suppression of turbulence by a uniform magnetic field. J. Fluid Mech. 28 (03), 571–592.

Muck, B., G ¨ unther, C., M ¨ uller, U. & B ¨ uhler, L. ¨ (2000) Three-dimensional mhd flows in rectangular ducts with internal obstacles. J. Fluid Mech. 418, 265–295.

Mutschke, G., Gerbeth, G., Shatrov, V. & Tomboulides, A. (1997) Two-and three-dimensional instabilities of the cylinder wake in an aligned magnetic field. Phys. Fluids 9, 3114.

Pothérat, A. (2007). Quasi-two-dimensional perturbations in duct flows under transverse magnetic field. Physics of Fluids, 19(7), 074104.

Rhodes, T. J., Smolentsev, S., & Abdou, M. (2018). Magnetohydrodynamic pressure drop and flow balancing of liquid metal flow in a prototypic fusion blanket manifold. *Physics of Fluids*, *30*(5), 057101.

Roshko A. (1993) Perspectives on bluff body aerodynamics. J. Wind Ind. Aerodyn. 49:79.

Sapardi, A.M., Hussam, W.K., Potherat, A. & Sheard, G.J. (2014) Three-dimensional linear stability analysis of the flow around a sharp 180 degree bend. In The Proceedings of the 19th Australasian Fluid Mechanics Conference (Eds: H. Chowdhury & F. Alam, Pub: Australasian Fluid Mechanics Society, ISBN: 978-0-646-59695-2), Paper 222. Conference: The 19th Australasian Fluid Mechanics Conference, RMIT University, 8-11 December 2014.

Sapardi, A.M., Hussam, W.K., Potherat, A. & Sheard, G.J. (2015) Influence of strong spanwise magnetic field on the quasi-two-dimensional MHD flow in a 180-degree sharp bend. In Proceedings of the Eleventh International Conference on Computational Fluid Dynamics in the Minerals and Process Industries (Eds: C.B. Solnordal, P. Liovic, G.W. Delaney, S.J. Cummins, M.P. Schwarz & P.J. Witt, Pub: CSIRO, Australia, ISBN: 978-1-4863-0620-6), 160SAP. Conference: The Eleventh International Conference on CFD in the Minerals and Process Industries, Melbourne Convention and Exhibition Centre, Melbourne, Australia, 7-9 December 2015.

Sapardi, M. A. M. (2018). *Hydrodynamic and Magnetohydrodynamic Flows Around a 180-Degree Sharp Bend* (Doctoral dissertation, Monash University).

Singh, M. K. (2017). Applications of Fluid Dynamics: An Introduction. Applications of Fluid Dynamics: Proceedings of ICAFD 2016.

Singh, R. J., & Gohil, T. B. (2019). The numerical analysis on the development of Lorentz force and its directional effect on the suppression of buoyancy-driven flow and heat transfer using OpenFOAM. *Computers & Fluids*, *179*, 476-489.

Smirnov, V. P. (2009). Tokamak foundation in USSR/Russia 1950–1990. *Nuclear fusion*, *50*(1), 014003.

Sommeria, J., & Moreau, R. (1982). Why, how, and when, MHD turbulence becomes two-dimensional. *Journal of Fluid Mechanics*, *118*, 507-518.

Verma, P. L., & Govardhan, M. (2011). Flow behind bluff bodies in side-by-side arrangement. *Journal of Engineering Science and Technology*, *6*(6), 745-768.

Weller, H. G., Tabor, G., Jasak, H., & Fureby, C. (1998). A tensorial approach to computational continuum mechanics using object-oriented techniques. *Computers in physics*, *12*(6), 620-631.

Zikanov, O., Krasnov, D., Boeck, T., Thess, A., and Rossi, M. (April 25, 2014). "Laminar-Turbulent Transition in Magnetohydrodynamic Duct, Pipe, and Channel Flows." ASME. *Appl. Mech. Rev*. May 2014; *66*(3): 030802. https://doi.org/10.1115/1.4027198

LIST OF PUBLICATIONS

Baharin, N. M. K., Sapardi, M. A. M., Hamid, A. H. A., & Bakar, S. N. S. A. (2021). Study on Flow Structure Behind Multiple Circular Cylinders in a Tandem Arrangement Under the Effect of Magnetic Field. *CFD Letters*, *13*(11), 126-136.

Baharin, N. M. K., Sapardi, M. A. M., Ab Razak, N. N., Hamid, A. H. A., & Bakar, S. N. S. A. (2021). Study on Magnetohydrodynamic Flow Past Two Circular Cylinders in Staggered Arrangement. *CFD Letters*, *13*(11), 65-77.

Hassim, M. R., Sapardi, M. A. M., Baharin, N. M. K., Bakar, S. N. S. A., Abdullah, M., & Nor, K. A. M. (2021). CFD Modelling of Wake-Induced Vibration At Low Reynolds Number. *CFD Letters*, *13*(11), 53-64.

DR. MOHD AZAN MOHAMMED SAPARDI
Assistant Professor
Department of Mechanical Engineering
Kulliyyah of Engineering
International Islamic University Malaysia